NASA CONTRACTOR REPORT

NASA CR-2269

NASA CR-2269

A NUMERICAL SOLUTION FOR THERMOACOUSTIC CONVECTION OF FLUIDS IN LOW GRAVITY

by L. W. Spradley, S. V. Bourgeois, C. Fan, and P. G. Grodzka

Prepared by
LOCKHEED MISSILES AND SPACE COMPANY, INC.
HUNTSVILLE RESEARCH AND ENGINEERING CENTER
Huntsville, Ala.
for George C. Marshall Space Flight Center

NATIONAL AERONAUTICS AND SPACE ADMINISTRATION • WASHINGTON, D. C. • MAY 1973

TECHNICAL REPORT STANDARD TITLE PAGE

1 REPORT NO.	2. GOVERNMENT ACCESSION NO.	3. RECIPIENT'S CATALOG NO.
NASA CR-2269		

4 TITLE AND SUBTITLE	5. REPORT DATE
A NUMERICAL SOLUTION FOR THERMOACOUSTIC CONVECTION OF FLUIDS IN LOW GRAVITY	May 1973
	6. PERFORMING ORGANIZATION CODE M456
7 AUTHOR(S) L.W. Spradley, S.V. Bourgeois, C. Fan, and P.G. Grodzka	8. PERFORMING ORGANIZATION REPORT # LMSC-HREC TR D306140
9 PERFORMING ORGANIZATION NAME AND ADDRESS Lockheed Missiles and Space Company, Inc. Huntsville Research and Engineering Center 4800 Bradford Drive Huntsville, Alabama	10. WORK UNIT NO.
	11 CONTRACT OR GRANT NO. NAS 8-27015
12. SPONSORING AGENCY NAME AND ADDRESS National Aeronautics and Space Administration Washington, D. C. 20546	13. TYPE OF REPORT & PERIOD COVERED Contractor
	14. SPONSORING AGENCY CODE

15 SUPPLEMENTARY NOTES

16. ABSTRACT

This report presents a finite difference numerical technique for solving the differential equations which describe thermal convection of compressible fluids in low gravity. Results of one-dimensional calculations are presented, and comparisons are made to previous solutions. The primary result presented is a one-dimensional radial model of the Apollo 14 Heat Flow and Convection Demonstration flight experiment. The numerical calculations show that thermally induced convective motion in a confined fluid can have significant effects on heat transfer in a low-gravity environment.

17 KEY WORDS	18. DISTRIBUTION STATEMENT

19 SECURITY CLASSIF (of this report)	20. SECURITY CLASSIF (of this page)	21 NO. OF PAGES	22. PRICE
Unclassified	Unclassified	90	$3.00

For sale by the National Technical Information Service, Springfield, Virginia 22151

FOREWORD

This report was prepared for the National Aeronautics and Space Administration, Marshall Space Flight Center, as a summary report on one phase of the work on Contract NAS8-27015, "Convection in Space Processing." The work described herein was performed in the Fluid Mechanics Section of the Lockheed-Huntsville Research & Engineering Center, John W. Benefield, Supervisor.

The NASA Contracting Officer's Representative for this work is Mr. T. C. Bannister, MSFC Space Sciences Laboratory (S&E-SSL-T).

ACKNOWLEDGEMENT

A special acknowledgment is due T. C. Bannister of NASA for his continuing interest and support of this and other space processing tasks.

CONTENTS

CONTENTS (Continued)

LIST OF ILLUSTRATIONS

NOMENCLATURE

Symbol	Description
c	speed of sound
C_p	specific heat at constant pressure
C_v	specific heat at constant volume
$\vec{F}$	body force vector
g	gravitational acceleration
i	node point "i" on finite-difference grid
k	thermal conductivity
K	coefficient of isothermal compressibility
L	characteristic length
n	time point "n" in finite-difference grid
Nu	Nusselt number
P	pressure
Pr	Prandtl number
q	total heat flux
$\vec{q}_r$	radiation heat flux vector
q_e	internal heat generation rate
R	gas constant
Re	Reynolds number
r	radial corrdinate
s	time scale factor
t	time
u	velocity component in x-direction (or r direction)
$\vec{V}$	velocity vector
x	Cartesian coordinate

NOMENCLATURE (Continued)

Symbol	Description
α	thermal diffusivity
β	coefficient of thermal expansion
γ	ratio of specific heats (C_p/C_v)
λ	"second" or bulk coefficient of viscosity
μ	dynamic viscosity
ρ	density
ϕ	viscous dissipation function
ν	kinematic viscosity

Subscript

o	initial condition or reference value
e	condition at earth's 1-g acceleration
w	wall condition
i	space coordinate designation in finite difference grid
m	mean value

Superscripts

n	time coordinate designation in finite difference grid
$'$	indicates dimensional quantities

Operators

$\frac{\partial}{\partial t}$	time partial derivative
$\frac{\partial}{\partial x}, \frac{\partial}{\partial r}$	space partial derivative
$\frac{D}{Dt}$	substantial derivative: $\frac{\partial}{\partial t} + (\vec{V} \cdot \nabla)$
	dot product of vectors
∇	gradient operator
∇	divergence operator
$\times$	cross product of vectors

Section 1
INTRODUCTION AND SUMMARY

The major advantage foreseen in manufacturing products in space is the near-absence of gravity. It may eventually prove feasible, in this unique environment, to produce products which are superior in quality to those made on earth. In manufacturing processes involving confined fluids which are heated, the low gravity environment of space should virtually eliminate natural fluid convection driven by gravity. However, there are driving forces other than gravity which could possibly produce significant fluid circulation in confined systems. If a free liquid surface is present, surface tension gradients due to temperature variations can induce convection. Thermally induced expansions and compressions in a confined gas could also generate fluid circulation. Convection driven by mechanisms other than gravity has received very little attention to date; thus the current effort was initiated to determine the magnitude and effects of non-gravity convection on typical space manufacturing processes.

The basic approach used to analyze this problem is to formulate a mathematical model of a simple yet representative system and obtain solutions for typical boundary conditions. The trends and magnitudes of non-gravity convection can then be estimated. The sample problem chosen is that of a single component compressible fluid in a low-gravity confined region which is heated along a wall. A one-dimensional flow situation is assumed and the governing partial differential equations are developed from the full equations for conservation of mass, momentum and energy. Since these are highly nonlinear and strongly coupled equations, a numerical solution utilizing finite-differences is employed. An explicit finite-difference scheme is used to program the equations on a Univac 1108 digital computer. Sample problems are solved in which thermally induced wave motion and heat conduction are included. Results have been obtained which indicate that pressure and thermal expansion effects can induce significant fluid motion and increase heat transfer in low gravity. In

addition, the pressure waves are confirmed to be acoustical as discussed in the literature. From the study it is concluded that non-gravity-driven thermo-acoustic convective motion in a compressible fluid could have significant effects on space manufacturing processes involving heated fluids. A recommendation is given for developing a two-dimensional analytic model for further study of pressure and thermal expansion convection in low gravity.

Section 2 of this report details the analytic formulation of the problem including the conservation equations, boundary conditions, dimensional analysis and assumptions. A discussion of the numerical solution method and finite-difference equations is given in Section 3. Appendixes A and B discuss the computer program which implements the numerical algorithms. Section 4 presents numerical results for two sample configurations — infinite parallel plates and concentric cylinders. Results for a one-dimensional radial model of the Apollo 14 Heat Flow and Convection Demonstration are also given. Conclusions are drawn from the results and recommendations for further analysis are given in Section 5.

Section 2
ANALYTIC DEVELOPMENT

2.1 THE PROBLEM

In conjunction with NASA's Manufacturing in Space Program, several demonstration experiments have flown aboard Apollo spacecraft on their moon missions. The Heat Flow and Convection Demonstration Experiments (Ref. 1) were flown on the Apollo 14 mission to obtain data and information on heat transfer and fluid behavior in a low-gravity environment. A similar experiment package has recently flown on the Apollo 17 mission. The results of the Apollo 14 experiments strongly indicate that some mode of fluid convection occurs even in a 10^{-6} to 10^{-4} g environment. The radial cell portion of these experiments exhibits a particularly interesting behavior. The "radial cell" consists of a cylinder of CO_2 gas which is heated at the center of the cylinder. Liquid crystals were used as temperature indicators. A theoretical heat transfer model of this unit was designed which includes conduction and radiation-but no fluid motion. A comparison of the theoretical model temperature predictions with the actual flight data is shown in Fig. 1 taken from Ref. 1. Although the magnitude of the numbers are in "reasonable" agreement, the shape of the flight data curve indicates that fluid convection was probably occurring. This curve rises faster at the early times than the pure conduction curve and then levels off while the conduction curve continues to rise. Reference 1 provides more details on these experiments.

The current analytic study of thermal convection was initiated to explain the behavior of the Apollo 14 radial cell data and to develop the analytical capability necessary to assess the role of low-gravity convection in space manufacturing processes.

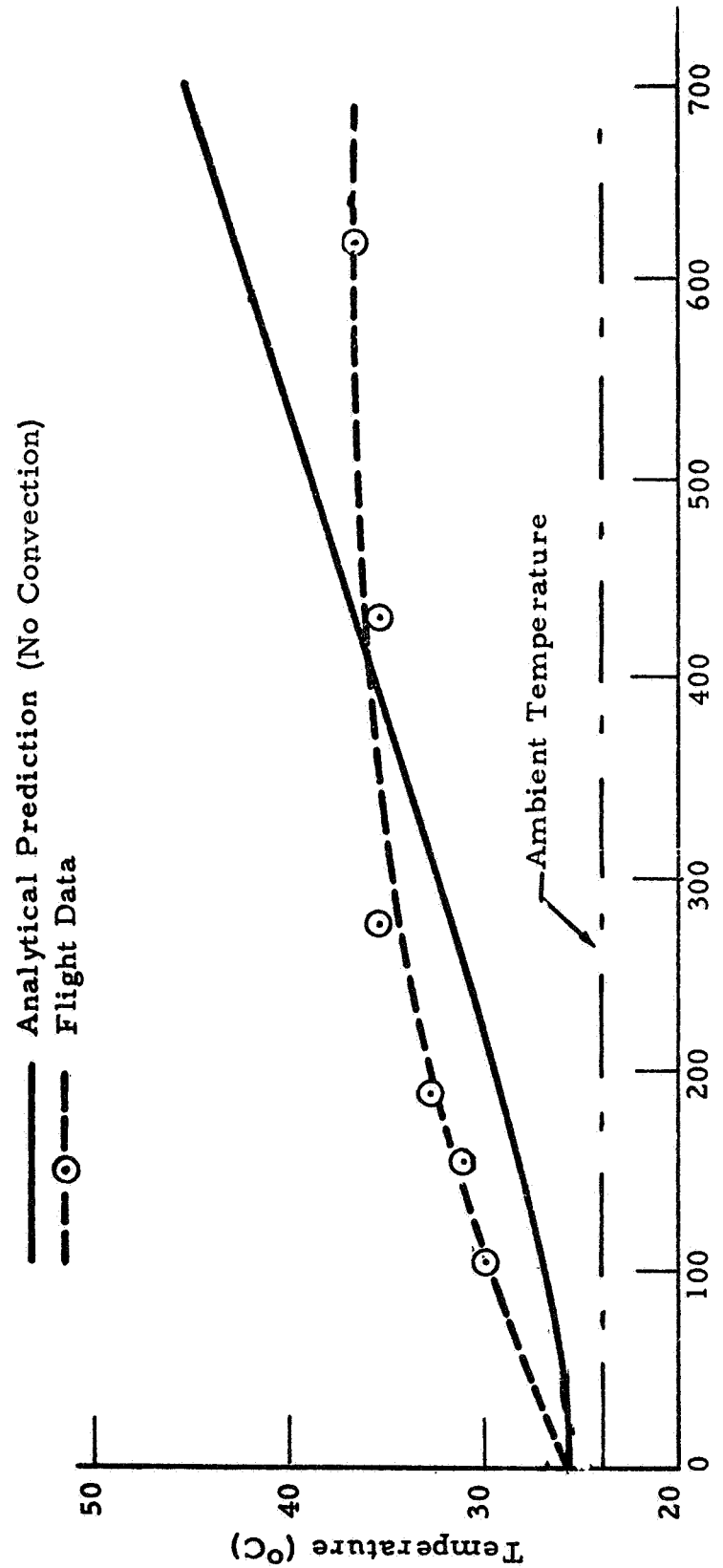

Fig. 1 — Typical Radial Heating Unit Temperature Profiles Comparing Theoretical Model to Flight Data (from Ref. 1)

2.2 ANALYTICAL APPROACH

The first step taken in this analysis was to postulate a possible driving mechanism for thermal convection of a completely confined compressible fluid in a low-gravity environment. The mechanism isolated for study here is the pressure and thermal expansion effects which result when a confined compressible fluid is heated. This problem, herein termed thermoacoustic convection, has received little attention in the literature. Trilling (Ref. 2), Knudsen (Ref. 3) and Luikov and Berkovsky (Ref. 4) used a linear perturbation analysis to investigate the wave motion induced in gases by boundary temperature gradients. They found that sharp rises in boundary temperature can induce expansions which cause pressure waves to propagate through the fluid in much the same manner as pushing a piston through a gas filled pipe. Larkin (Ref. 5) investigated the thermal expansion effects in a confined gas in zero gravity. He solved the nonlinear conservation equations, with compressibility effects, using a finite-difference numerical scheme on a digital computer. His results indicate that heat transfer rates and pressure rises are significantly increased over predictions which neglect the thermally induced fluid motion. His calculations confirmed the acoustic nature of the velocity waves. More recently, Thursaisamy (Ref. 6) reached similar conclusions while investigating pressure behavior in spacecraft cryogenic tanks.

The approach taken in this analysis is to formulate a mathematical model of a simple yet representative fluid system and to study solutions for typical boundary conditions encountered in "space manufacturing." The fluid mechanics model begins with the conservation equations of motion, continuity, and energy in Eulerian coordinates. For a viscous, heat conducting Newtonian fluid, these equations are found in standard text books (Refs. 7 and 8) in vector form:

Navier-Stokes Equation

$$\rho \frac{D\vec{V}}{Dt} = \vec{F} - \nabla P - \nabla \times \left[\mu (\nabla \times \vec{V})\right] + \nabla\left[(\lambda + 2\mu)\, \nabla \cdot \vec{V}\right] \qquad (1)$$

Continuity Equation

$$\frac{D\rho}{Dt} + \rho(\nabla \cdot \vec{V}) = 0 \qquad (2)$$

Energy Equation

$$\rho C_v \frac{DT}{Dt} = \frac{-\beta T}{K} (\nabla \cdot \vec{V}) + \nabla \cdot (k\nabla T) - \nabla \cdot \vec{q}_r + q_e + \phi \qquad (3)$$

Equation of State

$$P = P(\rho, T) \qquad (4)$$

These equations, with appropriate boundary conditions, describe the flow and thermal behavior of the fluid. These are, of course, highly nonlinear and strongly coupled equations such that general solutions are not possible. Appropriate assumptions and simplifications must be made if any solution to the convection problem is expected. Two models are used in this study to reduce the equations to a manageable form; however, the nonlinear behavior still renders analytic solutions impossible. A numerical solution utilizing finite-differences is employed.

2.3 MATHEMATICAL MODELS

Two flow models are considered. Both incorporate the same basic assumptions, but differ in geometric aspects. Model 1 consists of two infinite parallel plates which bound a compressible fluid. The flow situation is thus one-dimensional and can be described in a Cartesian reference frame. Model 2 consists of a radial segment of two concentric cylinders with a compressible gas between them. The outer cylinder then represents a fluid container and the inner cylinder is a heater. A one-dimensional radial coordinate system then describe the geometry. Both models utilize the following assumptions;

- Newtonian fluid obeying Stokes viscosity hypothesis ($\lambda = -2/3\mu$)
- Constant thermal properties k, C_v, μ, γ
- No radiation or internal heat sources
- No viscous dissipation of energy
- Body forces are negligible ($g/g_e << 1$)
- Ideal gas equation of state ($P = \rho RT$)

Most previous investigators have invoked the classical Boussinesq approximation which neglects the effects of pressure on the density profile and allows density to vary with temperature only in the body force term. The density is thus constant in all other terms resulting in a quasi-incompressible approach. This assumption is <u>not</u> made here. The equations of compressible flow are used with variable density in all terms and related to pressure and temperature through an ideal gas equation of state.

The primitive variable form of the equations are used as opposed to invoking transformations or combining equations to introduce fictitious variables. The modern literature, (e.g., Ref. 9), indicates that this approach may yield results which are more physically correct and also may have advantages in numerical stability and accuracy. The two mathematical models are now given.

2.3.1 Infinite Parallel Plate Model

The schematic below depicts the flow situation for Model 1.

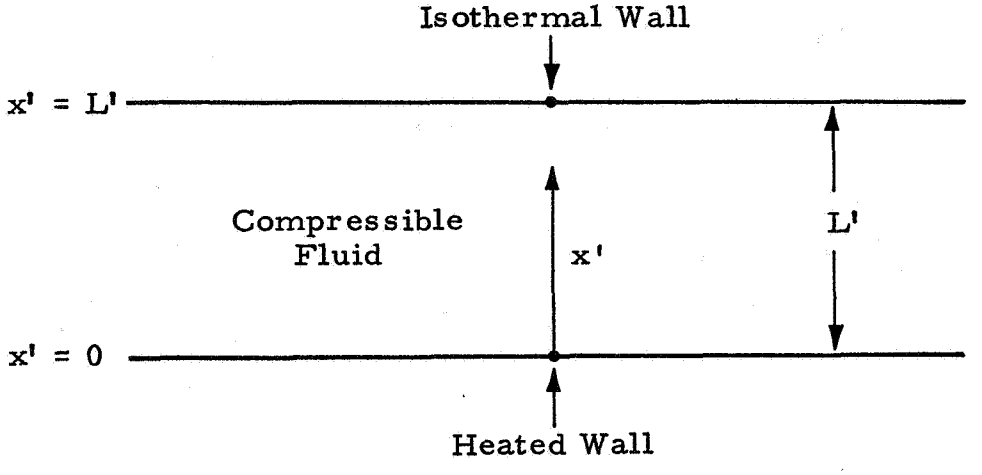

The governing equations (with the prescribed assumptions) can now be obtained from the general system (1) – (4). The one-dimensional Cartesian form is derived in most fluid mechanics texts (Refs. 7 and 8) and the derivation is not repeated here. Primes (') are used to indicate that a quantity has physical dimensions; unprimed variables are dimensionless. The governing equations take the following form:

Momentum

$$\frac{\partial}{\partial t'}(\rho' u') + \frac{\partial}{\partial x'}(\rho' u' u') = \frac{-\partial P'}{\partial x'} + 4/3\mu' \frac{\partial^2 u'}{\partial x'^2} \tag{5}$$

Continuity

$$\frac{\partial \rho'}{\partial t'} + \frac{\partial}{\partial x'}(\rho' u') = 0 \tag{6}$$

Energy

$$\rho' C_v' \frac{\partial T'}{\partial t'} + \rho' C_{v'} u' \frac{\partial T'}{\partial x'} = -P' \frac{\partial u'}{\partial x'} + k' \frac{\partial^2 T'}{\partial x'^2} \tag{7}$$

State

$$P' = \rho' R' T' \tag{8}$$

These equations will be nondimensionalized in Section 2.4 and expressed with dimensionless groups appearing as coefficients.

The intial and boundary conditions for Model 1 are expressed mathematically as follows:

Velocity

$$\left.\begin{aligned} u'(x', t'=0) &= 0 && \text{initially at rest} \\ u'(x'=0, t') &= u'(x'=L', t') = 0 && \text{no slip at walls} \end{aligned}\right\} \qquad (9)$$

Temperature

$$\left.\begin{aligned} T'(x', t'=0) &= T_o' && \text{initially isothermal} \\ T'(x'=0, t') &= T_w'(t') && \text{heated wall } x' = 0 \\ T'(x'=L', t') &= T_o && \text{isothermal wall } x' = L' \end{aligned}\right\} \qquad (10)$$

Pressure

$$\left.\frac{\partial P'}{\partial x'}\right|_{t'=0} = 0 \qquad \text{no body forces} \qquad (11)$$

Density

$$\rho'(x', t'=0) = \frac{P_o'}{R' T_o'} \qquad \text{equation of state} \qquad (12)$$

The thermal boundary condition at the heated wall is shown as a prescribed temperature history. This is done for simplicity of presentation. A prescribed heat flux boundary condition at $x = 0$ can also be used in Model 1 as seen later in Section 4.

Equations (5) through (12) formally define the mathematical Model 1 for analysis of thermoacoustic convection in low gravity.

2.3.3 Concentric Cylinder Radial Model

The schematic below depicts the flow situation for Model 2.

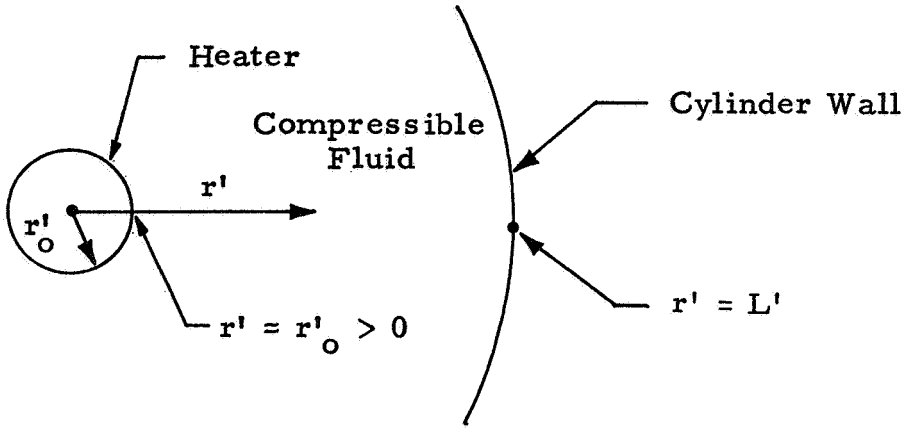

The governing equations for this configuration are again derived from the full system (1) – (4) (see Refs. 7 and 8). In terms of dimensional variables (') the equations take the following form.

Momentum

$$\frac{\partial}{\partial t'}(\rho' u') + \frac{1}{r'}\frac{\partial}{\partial r'}(r'\rho' u'u') = \frac{-\partial P'}{\partial r'} + 4/3\mu'\left[\frac{\partial^2 u'}{\partial r'^2} + \frac{1}{r'}\frac{\partial u'}{\partial r'} - \frac{u'}{r'^2}\right] \quad (13)$$

Continuity

$$\frac{\partial \rho'}{\partial t'} + \frac{1}{r'}\frac{\partial}{\partial r'}(r'\rho' u') = 0 \quad (14)$$

Energy

$$\rho' C_v' \frac{\partial T'}{\partial t'} + \rho' C_v' u' \frac{\partial T'}{\partial r'} = -P'\left[\frac{1}{r'}\frac{\partial}{\partial r'}(r'u')\right] + k'\left[\frac{\partial^2 T'}{\partial r'^2} + \frac{1}{r'}\frac{\partial T'}{\partial r'}\right] \quad (15)$$

State

$$P' = \rho' R' T' \tag{16}$$

The nondimensional form of these equations are actually used in the computation as in Model 1. Dimensional analysis is discussed in Section 2.4.

The initial and boundary conditions for Model 2 are expressed mathematically as follows:

Velocity

$$\left.\begin{aligned} &u'(r', t'=0) = 0 && \text{initially at rest} \\ &u'(r'=r_o', t') = u'(r'=L', t') = 0 && \text{no slip at walls} \end{aligned}\right\} \tag{17}$$

Temperature

$$\left.\begin{aligned} &T'(r', t'=0) = T_o' && \text{initially isothermal} \\ &\left\{\begin{aligned} &T'(r'=L', t) = T_o' \\ &\left.\frac{\partial T'}{\partial r'}\right|_{r'=L'} = 0 \end{aligned}\right. && \left\{\begin{aligned} &\text{isothermal wall} \\ &\text{or} \\ &\text{adiabatic wall} \end{aligned}\right. \end{aligned}\right\} \tag{18}$$

$$\left.\begin{aligned} &T'(r'=r_o', t') = T_w'(t') \\ &\left.\frac{\partial T'}{\partial r'}\right|_{r'=r_o'} = \frac{-q'}{k'} \end{aligned}\right\} \begin{aligned} &\text{prescribed temperature} \\ &\text{or} \\ &\text{prescribed heat flux} \end{aligned} \tag{19}$$

Pressure

$$\left.\frac{\partial P'}{\partial r'}\right|_{t'=0} = 0 \qquad \text{no body forces} \tag{20}$$

Density

$$\rho'(r', t'=0) = \frac{P_o'}{R' T_o'} \qquad \text{equation of state} \qquad (21)$$

Equations (13) through (21) formally define Model 2 for analysis of thermoacoustic convection in low gravity.

2.4 DIMENSIONAL ANALYSIS

Dimensional analysis is commonly used for a variety of scientific problems. It is basically a formal mathematical procedure which yields the dimensionless parameters associated with a particular problem. The procedures for performing dimensional analysis vary considerably among authors. Ostrach (Ref. 10) and Hellums and Churchill (Ref. 11) present two approaches for dimensional analysis of natural convection problems. There are two major uncertainties in choosing reference values for natural convection probelms — the characteristic time and characteristic velocity of these systems are not always obvious. Since the present problem involves acoustic velocity waves, the isothermal sound velocity of the gas is used as the characteristic velocity. The characteristic time used is the time required for a wave to travel the length of the container. This same reference velocity is also obtained using the method of Ostrach (Ref. 10) by equating the inertial forces and pressure forces in the momentum equation.

The following dimensionless variables are now introduced:

$$x = \frac{x'}{L'} \quad t = t' \frac{\sqrt{R' T_o'}}{L'} \quad r = \frac{r'}{L'} \quad T = \frac{T'}{T_o'} \quad u = \frac{u'}{\sqrt{R' T_o'}} \quad P = \frac{P'}{P_o'} \quad \rho = \frac{\rho'}{\rho_o'} \qquad (22)$$

Model 1 is used here to illustrate the dimensionless form of the differential equations. Model 2 is very similar and is not shown here, but is used in dimensionless form in all computation. The expressions in Eq. (22) are

substituted into Eqs. (5) through (8) and the boundary conditions Eqs. (9) through (12). Algebraic manipulation then yields the following dimensionless equations and boundary conditions.

Momentum (Dimensionless)

$$\frac{\partial}{\partial t}(\rho u) + \frac{\partial}{\partial x}(\rho uu) = \frac{-\partial P}{\partial x} + \frac{4}{3}\left(\frac{1}{Re}\right)\frac{\partial^2 u}{\partial x^2} \tag{23}$$

Continuity (Dimensionless)

$$\frac{\partial \rho}{\partial t} + \frac{\partial}{\partial x}(\rho u) = 0 \tag{24}$$

Energy (Dimensionless)

$$\rho\frac{\partial T}{\partial t} + \rho u\frac{\partial T}{\partial x} = -(\gamma-1)P\frac{\partial u}{\partial x} + \left(\frac{\gamma}{Re\ Pr}\right)\frac{\partial^2 T}{\partial x^2} \tag{25}$$

State (Dimensionless)

$$P = \rho T \tag{26}$$

Initial Conditions (Dimensionless)

$$u(x, t=0) = 0 \qquad T(x, t=0) = 1 \qquad \rho(x, t=0) = 1 \tag{27}$$

Boundary Conditions (Dimensionless)

$$\begin{aligned} &u(x=0, t) = u(x=1, t) = 0 \\ &T(x=0, t) = T_w(t) \\ &T(x=1, t) = 1 \end{aligned} \tag{28}$$

The dimensionless groups which appear in the equations are:

$$\text{Prandtl Number } Pr = \frac{\mu' C_p'}{k'} \qquad \frac{\text{Momentum Diffusion}}{\text{Thermal Diffusion}}$$

$$\text{Reynolds Number } Re = \frac{L' \sqrt{R' T_o'}\, \rho_o'}{\mu'} \qquad \frac{\text{Inertial Forces}}{\text{Viscous Forces}} \tag{29}$$

$$\text{Peclet Number } Pe = Re \cdot Pr \qquad \frac{\text{Convection}}{\text{Conduction}}$$

$$\text{Ratio of specific heats } \gamma = \frac{C_p'}{C_v'}$$

For the present problems of interest, γ and Pr are of order O(1) and Re is $O(10^6)$. This dimensionless form of the equations is used in all numerical computation.

This completes the formal development of the mathematical models used in this study of thermal convection in low gravity. The numerical solution algorithms are now presented.

Section 3
NUMERICAL SOLUTION METHOD

3.1 METHODS SURVEY

The following brief review of the literature is not intended to be a complete survey; only the work more pertinent to the present problem is reviewed. Many excellent articles were examined during this study, but only those directly related to the current problem of numerical computation of natural convection are presented here.

Hellums and Churchill (Refs. 12 and 13) have applied finite difference calculations to natural convection for several types of problems. Explicit, time-dependent finite difference approximations were made to the conservation equations for mass, momentum and energy. Gravity was the only driving force considered. This work has pointed out that any method which is to be used on a computer should undergo a rigorous stability analysis and that the convection terms must be handled with much care. The Hellums-Churchill technique uses alternating forward and backward differences depending on the direction of the fluid flow. Computer storage and run time were found to be moderate. Agreement with previous results was excellent in some regions and good in others.

Fromm (Ref. 14) presents some numerical results for the Bénard problem of heating a fluid layer from below in a gravity field. The classical Boussinesq approximation is made and the governing equations are transformed to the vorticity-stream-function form. Central finite differences are used in the numerical solution algorithm. Cases examined include Rayleigh numbers from the critical value to $Ra = 10^7$. Correlations of heat transport with Rayleigh number are given and excellent comparisons are made with previous analysis and experiments.

Clark and Barakat (Ref. 15) have applied numerical computation to the problem of two-dimensional, laminar, transient, natural convection of a fluid in a rectangular container with a free surface. Explicit finite difference methods were applied with success to the problem of a vapor-liquid interface. They concluded, however, that implicit methods may be preferred if only steady state results are needed. The theoretical results are compared to experimental measurements from the literature and indicate qualitative agreement.

Wilkes and Churchill (Ref. 16) studied natural convection of a fluid contained in a long horizontal enclosure of rectangular cross section. Two-dimensional motion was assumed. The vorticity and energy equations were solved numerically by alternating direction finite difference methods. Compressibility effects were neglected, the density was allowed to vary only in the buoyancy term, and gravity was the only driving mechanism considered. Numerical results for several cases (heating from the side) were compared to experiment with good agreement. Their results demonstrate that finite difference methods can adequately simulate the thermal convection problem of heating from the side.

Larkin (Ref. 17) gives a brief but important discussion of the numerical conservation principles which must be observed in solving the continuity equation. He presents an implicit technique which preserves an overall mass balance in a closed system. It is easy to implement due to the tridiagonal form of the coefficient matrix.

Samuels and Churchill (Ref. 18) used finite difference methods to compute hydrodynamic instability due to convection in a horizontal rectangular region heated from below. Critical Rayleigh numbers were determined for a series of Prandtl numbers and length-to-height ratios. One of the major objectives of the work was to assess the usefulness of finite difference techniques for computation of natural convection. The governing equations were transformed such that a vorticity equation and an energy equation were treated and an implicit alternating direction finite difference method was used to solve the equations. Calculated

critical Rayleigh numbers were found to be in excellent agreement with other analytical results for Prandtl numbers greater than unity. For Prandtl numbers less than unity, the calculated critical Rayleigh numbers exhibited a dependence on Prandtl number, a fact not predicted by linearized theory. If symmetrical initial conditions were imposed, a non-unique set of solutions were obtained. However, if an asymmetric initial condition was imposed, the calculation always converged to a single unique flow pattern.

Aziz and Hellums (Ref. 19) present results of numerical calculation of three-dimensional laminar natural convection. The complete Navier-Stokes equations are transformed and expressed in terms of vorticity and a vector potential. A finite-difference method using alternating directions is used for the parabolic equations (vorticity and temperature) and a successive over-relaxation technique is applied to the elliptic stream function equation. Comparisons with previous works for two-dimensional problems are made and the conclusion is reached that the authors' method has important advantages in speed and accuracy. This is the most complete work that has been found on the three-dimensional natural convection problem.

Torrance (Ref. 20) presents an excellent summary, review and comparison of finite-difference computations of natural convection. Five numerical methods, were compared for calculating two-dimensional transient natural convection in an enclosure. Both implicit and explicit procedures were considered. Consideration was given to stability, accuracy and conservation of each method and it was concluded that no one method has all the features that are desirable. An explicit procedure developed by Torrance was shown to be conservative and stable without a restriction on the spatial mesh increment. A tentative conclusion reached by Torrance is that, (1) the Dufort-Frankel method will require less computer time if the mesh size restriction can be satisfied, (2) the Torrance method should be used if the results are interpreted in the sense of a large truncation error. The paper presents an excellent comparison chart of the type of difference forms which various authors have used.

Plows (Ref. 21) presents numerical solutions for the laminar Bénard problem. The Boussinesq-type equations are solved by a numerical scheme utilizing centered "leapfrog" differences for first order derivatives and a Dufort-Frankel pattern for second derivatives. An iterative scheme is used to determine Nusselt numbers and roll patterns for Rayleigh numbers between 2000 and 22,000 for a range of Prandtl numbers. Nusselt number versus Rayleigh number calculations are presented and compare favorably with previous analytical and experimental studies.

Schwab and DeWitt (Ref. 22) conducted a numerical investigation of free convection between two vertical coaxial cylinders. The coupled, nonlinear, partial differential equations were converted to finite-difference form and solved using an alternating direction implicit procedure. Results, in the form of steady state contour maps, are presented for several combinations of Prandtl and Grashof numbers. Among the conclusions reached is that a fully developed boundary layer flow was found to exist in the cavity for Rayleigh numbers greater than 5×10^3. The variation of steady state Nusselt numbers with Prandtl and Rayleigh numbers and with geometric ratios was also briefly discussed.

Cabelli and DeVahl Davis (Ref. 23) present a numerical study of the Bénard cell problem for the case where buoyancy and surface tension are coupled. The conservation equations are expressed in the vorticity-stream function form and a surface tension boundary condition is imposed on the free surface. The vorticity and energy equation were solved with an alternating direction implicit finite-difference scheme and the stream-function equation was solved by over-relaxation. This appears to be the first work to solve the full conservation equations with surface tension effects coupled to buoyancy. The numerical results indicate that surface tension effects encourage the natural fluid motion in liquids. The reader is referred to this reference for details of their calculations.

Heinmiller (Ref. 24) has developed a mathematical model of thermal stratification and natural convection occurring in supercritical oxygen under

low-gravity environments. His model uses an explicit finite difference solution of the primitive equations for conservation of mass, momentum and energy. The Boussinesq assumption is not made and real gas properties are used throughout the computation. This work appears to be among the first to solve the full compressible form of the equations for a two-dimensional problem. The numerical model was used to successfully simulate a pressure collapse in the Apollo 12 oxygen storage system due to an acceleration change.

Barton et al. (Ref. 25) also developed a numerical model for analysis of the Apollo spacecraft oxygen tank system. A numerical algorithm known as the General Elliptic Method (GEM) is developed for solution of the full conservation equations in terms of the primitive variables. This method was also applied with success to the Apollo oxygen tank stratification problem.

Thuraisamy (Ref. 6) presents a detailed one-dimensional model of natural convection in zero gravity. His aim was to analyze the flow of supercritical oxygen in the Apollo tanks. His model is a one-dimensional radial segment through two concentric cylinders – the outer cylinder being a tank wall and the inner cylinder being a heater. The model includes pressure and thermal expansion effects which are the subject of this report. Details of this work will be given in Section 4 where comparisons with present calculations are given.

Larkin (Ref. 5) was the first to apply numerical computation to the governing equations including compressibility effects. He considered the one-dimensional flow of a perfect gas in a zero gravity confined container. Explicit finite differences were used on the momentum and energy equations and an implicit method was applied to the continuity equation. The results show that the pressure wave motion is acoustical in nature. Heating rates and pressure rise are greatly increased over those obtained with conduction alone. Larkin's analysis will be detailed in Section 4 and comparisons will be made to the present work.

A study of other applicable numerical methods was made during this literature survey. Textbooks such as Refs. 26 and 27 are excellent for general problems but application to thermal convection is lacking. References 9 and 28 through 30 contain a variety of finite difference techniques for application to general fluids problems. Cheng (Ref. 9) presents an excellent discussion of the conservation law approach to the numerical solution of the Navier-Stokes equations. Lax and Wendroff (Ref. 28) also discusses the conservation law form for solution of hyperbolic equations. Campbell (Ref. 29) presents a stability analysis for a finite difference solution to the Navier-Stokes equations. Brunson and Wellek (Ref. 30) present a mathematical discussion of the numerical stability of a Dufort-Frankel scheme for solving systems of parabolic equations.

3.2 FINITE-DIFFERENCE EQUATIONS

An explicit finite difference scheme will be applied to the present thermal convection problem. The unsteady form of the equations are used to study the transient behavior of the problem. The explicit approach with the unsteady equations allows a forward-marching-in-time algorithm to be employed. Forward time differences are used on the unsteady terms and space-centered differences are used on all space derivatives except the convection terms where a "flip-flop" forward-backward scheme is used. Although this scheme is only first-order, it should be sufficiently accurate for the qualitative result sought here. This was verified by comparing results to a second-order Dufort-Frankel algorithm (see Appendix B). The explicit formulation was chosen primarily because it is simple, easy to program and is non-iterative in nature.

A node centered spatial mesh, shown in the schematic on the next page, is used to write the difference equations. In this grid, x_i denotes space point i; $x_i = (i - 1/2)\Delta x$. The grid spacing Δx is constant.

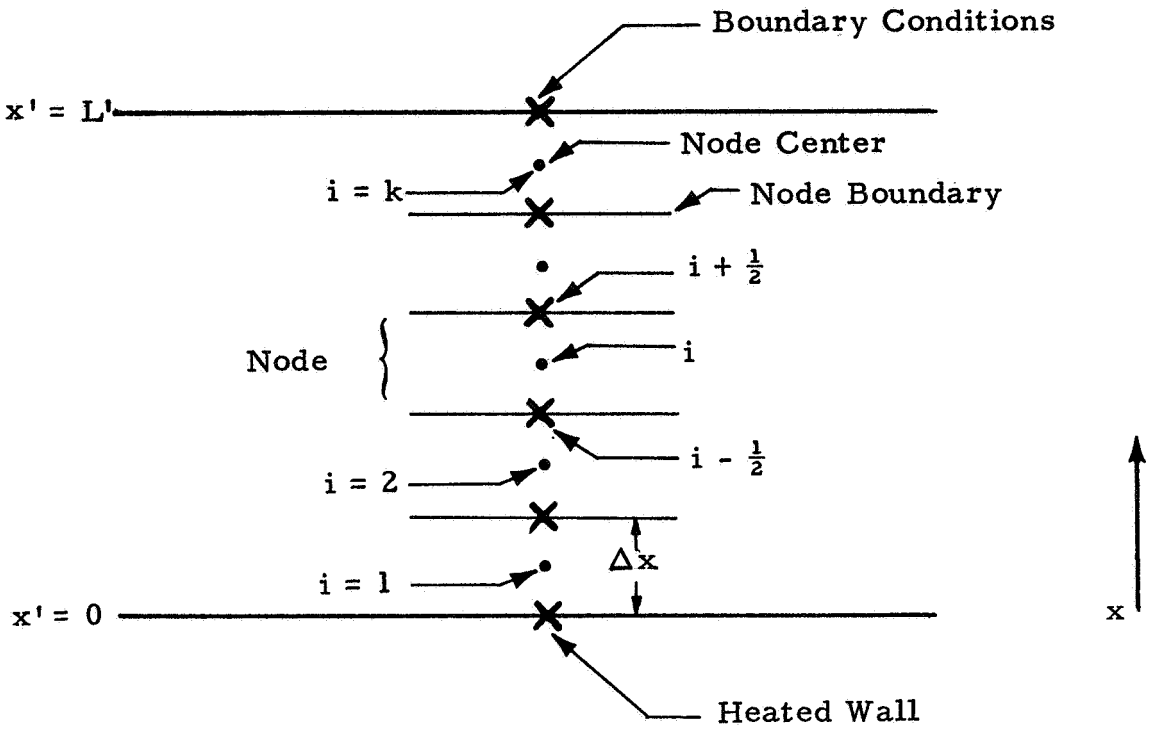

All quantities, (u, ρ, T, P), are defined at node centers, and differences are taken across a node using the "half-increment" quantities. This approach offers better conservation features than a scheme based on mixed node-center/node-boundary differences. A similar grid system was used by Heinmiller (Ref. 24). The half-increment quantities are defined at node boundaries by interpolation over node centered variables, i.e.,

$$\rho_{i+\frac{1}{2}} = \tfrac{1}{2}(\rho_i + \rho_{i+1})$$
$$u_{i-\frac{1}{2}} = \tfrac{1}{2}(u_i + u_{i-1}) \qquad (32)$$

Time derivatives are approximated by forward differences as follows:

$$\frac{\partial T}{\partial t} \approx \frac{T_i^{n+1} - T_i^n}{\Delta t} \qquad (33)$$

Where i denotes space point x_i, n denotes time t_n and n+1 denotes the new time t_{n+1}. First order space derivatives except convection terms are approximated by central differences,

$$\frac{\partial P}{\partial x} \approx \frac{P^n_{i+1} - P^n_{i-1}}{2\Delta x} \tag{34}$$

Second order space derivatives are approximated by the usual centered form;

$$\frac{\partial^2 u}{\partial x^2} \approx \frac{u^n_{i+1} - 2u^n_i + u^n_{i-1}}{(\Delta x)^2} \tag{35}$$

The convection terms must be handled in a special manner in the explicit approach. If space-centered differences are used, the method becomes unstable regardless of the step sizes (Ref. 26). Hellums and Churchill (Ref. 12) and Larkin (Ref. 5) have used the following "flip-flop" method successfully.

$$u\frac{\partial T}{\partial x} \approx \begin{cases} u^n_i \left(\dfrac{T^n_{i+1} - T^n_i}{\Delta x}\right) & \text{if } u^n_i < 0 \\ u^n_i \left(\dfrac{T^n_i - T^n_{i-1}}{\Delta x}\right) & \text{if } u^n_i > 0 \end{cases} \tag{36}$$

This forward-backward alternating direction scheme is used depending on the direction of the recirculating flow. Reference 12 shows that this method is conditionally stable. In the present work, the convective terms in the momentum and energy equations are differenced according to this scheme.

The explicit differencing of the continuity equation requires special attention. As pointed out by Larkin (Ref. 17), strict mass conservation

laws must be obeyed numerically if meaningful results are expected. However, the usual centered difference explicit method which would numerically conserve mass is unconditionally unstable. Larkin used an implicit method on this equation in order to bypass this restriction. In the present work, an explicit method similar to that of Heinmiller (Ref.24) was devised which is conditionally stable and conservative. The basis of the method is the use of the divergence form of the momentum and continuity equations. The momentum equation is solved first to yield the ρu product at the new time point. This ρu product at the new time is then central differenced in the continuity equation to yield the updated density ρ. The velocity is then computed from $(\rho u)/\rho$.

Special forms of the difference equations are used at the nodes adjacent to a wall. This is necessary for accurate handling of boundary conditions. For example;

$$\left.\frac{\partial^2 u}{\partial x^2}\right|_{\text{node 1}} \approx \frac{u_2^n - 3u_1^n}{(\Delta x)^2} \qquad (37)$$

Forms such as this are derived by computing node boundary points using linear interpolation and the differencing across the node using the known boundary conditions.

A complete listing of the difference forms used in this work are shown in figs. 2, 3 and 4 for the momentum, continuity and energy equations respectively. In this figure, i denotes space node x_i, n denotes time point t_n: (i=1 and i=k are the nodes adjacent to a wall). The finite difference equations are shown for Model 1 only since those for Model 2 are very similar.

A Dufort-Frankel numerical scheme was also developed during this study. Details are given in Appendix B.

Momentum Equation

$$\frac{\partial}{\partial t}(\rho u) + \frac{\partial}{\partial x}(\rho uu) = -\frac{\partial P}{\partial x} + 4/3\left(1/Re\right)\frac{\partial^2 u}{\partial x^2}$$

Finite Difference Form

$$(\rho u)_i^{n+1} = (\rho u)_i^n - \Delta t \left[\delta_x (\rho uu)_i^n + \delta_x (P)_i^n - \frac{4}{3}\left(\frac{1}{Re}\right)\delta_x^2 (u)_i^n \right]$$

Difference Equations

$$\left.\begin{aligned} \delta_x(\rho uu)_i^n &= \frac{(\rho u)_{i+1}^n \, u_{i+1}^n - (\rho u)_i^n \, u_{i-1}^n}{\Delta x} \qquad u_i^n < 0 \\ \delta_x(\rho uu)_i^n &= \frac{(\rho u)_i^n \, u_i^n - (\rho u)_{i-1}^n \, u_{i-1}^n}{\Delta x} \qquad u_i^n \geq 0 \end{aligned}\right\} \quad i = 2, \ldots, k-1$$

$$\delta_x(\rho uu)_1^n = \frac{(\rho u)_1^n \, u_1^n + (\rho u)_2^n \, u_2^n}{2\Delta x}$$

$$\delta_x(\rho uu)_k^n = \frac{-\left[(\rho u)_k^n \, u_k^n + (\rho u)_{k-1}^n \, u_{k-1}^n\right]}{2\Delta x}$$

$$\delta_x(P)_i^n = \frac{P_{i+1}^n - P_{i-1}^n}{2\Delta x} \qquad i = 2, \ldots, k-1$$

$$\delta_x(P)_1^n = \frac{P_2 - P_1}{\Delta x}$$

$$\delta_x(P)_k^n = \frac{P_k - P_{k-1}}{\Delta x}$$

$$\delta_x^2(u)_i^n = \frac{u_{i+1}^n - 2u_i^n + u_{i-1}^n}{(\Delta x)^2} \qquad i = 2, \ldots, k-1$$

$$\delta_x^2(u)_1^n = \frac{u_2^n - 3u_1^n}{(\Delta x)^2}$$

$$\delta_x^2(u)_k^n = \frac{u_{k-1}^n - 3u_k^n}{(\Delta x)^2}$$

Fig. 2 — Finite Difference Form of Momentum Equation

Continuity Equation

$$\frac{\partial \rho}{\partial t} = - \frac{\partial}{\partial x} (\rho u)$$

Finite Difference Form

$$\rho_i^{n+1} = \rho_i^n - \Delta t \left[\delta_x (\rho u)_i^{n+\frac{1}{2}} \right]$$

Difference Equations

$$\delta_x (\rho u)_i^{n+\frac{1}{2}} = \frac{(\rho u)_{i+1}^{n+1} - (\rho u)_{i-1}^{n+1}}{2\Delta x} \qquad i = 2, \ldots k-1$$

$$\delta_x (\rho u)_1^n = \frac{(\rho u)_1^{n+1} + (\rho u)_2^{n+1}}{2\Delta x}$$

$$\delta_x (\rho u)_k^n = \frac{- \left[(\rho u)_k^{n+1} + (\rho u)_{k-1}^{n+1} \right]}{2\Delta x}$$

$$u_i^{n+1} = (\rho u)_i^{n+1} / \rho_i^{n+1}$$

Fig. 3 - Finite Difference Form of Continuity Equation

Energy Equation

$$\frac{\partial T}{\partial t} + u\frac{\partial T}{\partial x} = -\frac{(\gamma-1)}{\rho} P \frac{\partial u}{\partial x} + \frac{\gamma}{\rho}\left(\frac{1}{Re\,Pr}\right)\frac{\partial^2 T}{\partial x^2}$$

Finite Difference Form

$$T_i^{n+1} = T_i^n - \Delta t \left[u_i^{n+1}\,\delta_x(T)_i^n + \frac{(\gamma-1)}{\rho_i^{n+1}} P_i^n\,\delta_x(u)_i^{n+1} - \frac{\gamma}{\rho_i^{n+1}}\left(\frac{1}{Re\,Pr}\right)\delta_x^2(T)_i^n\right]$$

Difference Equations

$$\delta_x(u)_i^{n+1} = \frac{u_{i+1}^{n+1} - u_{i-1}^{n+1}}{2\Delta x} \qquad i = 2, \ldots, k-1$$

$$\delta_x(u)_1^{n+1} = \frac{u_1^{n+1} + u_2^{n+1}}{2\Delta x} \qquad \delta_x(u)_k^{n+1} = -\frac{\left[u_k^{n+1} + u_{k-1}^{n+1}\right]}{2\Delta x}$$

$$\delta_x(T)_i^n = \begin{cases} \dfrac{T_{i+1}^n - T_i^n}{\Delta x} & u_i^n < 0 \\ \dfrac{T_i^n - T_{i-1}^n}{\Delta x} & u_i^n \geq 0 \end{cases} \qquad i = 2, \ldots, k-1$$

$$\delta_x(T)_1^n = \begin{cases} \dfrac{T_2^n - T_1^n}{\Delta x} & u_1 < 0 \\ \dfrac{T_1^n - T_w^n}{\frac{1}{2}\Delta x} & u_1 \geq 0 \end{cases} \qquad \delta_x(T)_k^n = \begin{cases} \dfrac{T_k^n - T_{k-1}^n}{\Delta x} & u_k \geq 0 \\ \dfrac{T_0^n - T_k}{\frac{1}{2}\Delta x} & u_k < 0 \end{cases}$$

$$\delta_x^2(T)_i^n = \frac{T_{i+1}^n - 2T_i^n + T_{i-1}^n}{(\Delta x)^2} \qquad i = 2, \ldots, k-1$$

$$\delta_x^2(T)_1^n = \frac{T_2^n - 3T_1^n + 2T_w^n}{(\Delta x)^2} \qquad \delta_x^2(T)_k^n = \frac{T_{k-1}^n - 3T_k^n + 2T_0^n}{(\Delta x)^2}$$

Fig. 4 - Finite Difference Form of Energy Equation

3.3 NUMERICAL STABILITY

The explicit finite difference scheme just presented is a conditionally stable method. If certain criteria are met, the difference equations that are solved will approximate the solution of the differential equations. If the stability criteria are not met, unrealistic solutions or no solutions at all will result. The stability criterion of this method is a restriction on the size of the time increment Δt. The stability of the method is free of a spatial mesh (Δx) restriction and only accuracy dictates the size of Δx.

The time step restriction for this method was determined by using the available literature and by experimenting numerically. This approach was necessary since a mathematical analysis of stability for nonlinear problems remains beyond the state of the art. For the present problem, in which pressure wave propagation contributes significantly, the time step should be determined by the time required for a pressure wave to propagate over a distance of one node length Δx, i.e.,

$$\Delta t' < \left[\frac{\Delta x'}{|u'| + c'} \right]_{min} \tag{38}$$

where c' is the velocity of sound. This is recognized as the familiar hyperbolic limit known as the CFL condition (Ref. 26). Numerical experiment has shown this to be the governing stability criteria for the present problem.

Since $|u'| << c'$ and $c' = \sqrt{\gamma R' T'}$ for a perfect gas, we have

$$\Delta t' < \left[\frac{\Delta x}{\sqrt{\gamma R' T'}} \right]_{min} \tag{39}$$

In terms of the dimensionless variables (Section 2.4) we get the following stability requirement.

$$\Delta t < \frac{\Delta x}{\sqrt{\gamma T_w}} \tag{40}$$

For moderate values of Δx, i.e., 20 mesh points, Δt is of the order of 0.01 which corresponds to about 10^{-4} seconds of real time. Even for a machine of the capability of the Univac 1108 this problem is not trivial in terms of run time. It may appear that an implicit procedure would relieve this time step restriction. Note, however, that it is still the physical phenomena of acoustic wave motion that restricts the time step size. An implicit method, using larger time steps, may bypass important physical behavior.

3.4 SCALING PRINCIPLES

A scaling procedure developed in Ref. 24 and used in Ref. 6 has been incorporated into the present numerical algorithm to lessen the severe time step requirement. This procedure is now briefly outlined including its applicability to the present problems and limitations on the magnitude of scaling which is permissible.

The basic problem arises because diffusion processes occur on a time scale much larger than that of acoustic wave motion. The purpose of scaling is to speed up certain of the physical processes occurring in the fluid without disturbing the thermodynamic state of the fluid itself. The following procedure is based on familar similarity laws of fluid mechanics (Ref. 8). The dimensionless groups which apply to the present problem are:

$$\text{Reynolds number } Re = \frac{\rho' L' u'}{\mu'}$$

$$\text{Prandtl number } Pr = \frac{\mu' C_p'}{k'} \tag{41}$$

$$\text{Nusselt number } Nu = \frac{q' L'}{k' \Delta T'}$$

$$\text{Mach number } M = \frac{u'}{c'}$$

The objective is to increase the real time/computer time ratio by a factor of s such that each time step Δt that is used for computation will correspond to a real time s Δt. To achieve this objective, we define a flow situation, which is similar, but not perfectly equivalent, to our original problem, by the following transformations:

$$
\begin{aligned}
t' &= st'_s \\
\mu'_s &= s\mu' \\
k'_s &= sk' \\
q'_s &= sq' \\
u'_s &= su'
\end{aligned}
\tag{42}
$$

where the s subscript indicates a flow variable in a new time frame. We then have the thermal conductivity, viscosity, heat input and flow velocity increased by a factor of s. The new time frame t_s in which we compute will now correspond to real time, st. The thermodynamic state of the fluid, temperature, pressure and density, remain unchanged in the new time system. We must now note that each of the dimensionless groups in Eq. (41), except Mach number, are the same in both time frames. We have increased the Mach number by a factor of s since the properties of the fluid which determine the sonic velocity have been preserved. Since the sonic velocity is unchanged, the size of the permissible computation time step Δt_s is unchanged, but the real time Δt is increased. This satisfies our original objective.

We can assess the limitations on this scaling procedure by considering the differential Eqs. (5) and (7). The scaling method essentially multiplies the unsteady terms and the diffusion terms by a factor s, or equivalently dividing the convection terms by s. The procedure is thus valid for problems in which the convection terms are "small" relative to the other terms in the equations. The size of the factor s is then a function of the "smallness" of these convection terms. For s = 1 we have an exact simulation of the problem and as s approaches infinity, we approach as a limit the pure conduction solution for a compressible fluid.

In the present analysis, calculations are made both for problems in which the convection terms dominate and for problems in which they are relatively small. The size of the scale factor s used in actual calculations is discussed in Section 4 where some results for typical problems are given.

3.5 COMPUTER PROGRAM

The finite difference method given in Section 3.2 was programmed in FORTRAN V language for a Univac 1108 Exec 8 digital computer. The equations for Model 1 and Model 2 were coded in the same program, termed TC1, with optional flags to control the program flow. A driver program which calls subroutines is used to allow complete flexibility of use. All input and output is performed in separate subroutines and each of the four basic equations, momentum, continuity, energy and state, are coded in individual subroutines. All data are input with punched cards and all output data are in printed page format. Provisions for running a problem in parts (timewise) is included. Details of the TC1 program are given in Appendix A.

Section 4
DISCUSSION OF RESULTS

4.1 SCOPE OF RESULTS

This section summarizes the results which have been obtained to date for the one-dimensional models of thermoacoustic convection. The objectives of the sample calculations were to

- Qualitatively determine the importance of thermoacoustic effects as a heat transfer mechanism.
- Assist in the analysis of the data from the Apollo 14 Heat Flow and Convection Demonstration.
- Verify the numerical calculation method which may be used for analyzing other types of convection encountered in space processing.

These objectives are met by performing calculations, using the TCI program, for two representative problems. Case 1 consists of two infinite parallel plates with helium gas as the fluid. One wall is maintained isothermal and the other is subjected to an instantaneous temperature step. This case was chosen because; (1) solutions exist in the literature which can be used to verify the model and numerical method, and (2) this case should provide an upper limit on the severity of the thermal boundary conditions. Results for case 1 are compared and constrasted to those of Larkin (Ref. 5) and Thuraisamy (Ref. 6). The solution is shown to converge smoothly to an accurate steady steady given by an analytic expression. The importance of pressure convection is also established for this boundary condition.

Case 2 consists of a cylindrical configuration with carbon dioxide as the fluid. The dimensions of the container and the fluid properties correspond to those of the Apollo 14 Heat Flow and Convection Demonstration (HFC). The

reader should refer to Ref. 1 for details of the HFC experiment. Three types of thermal boundary conditions are applied to case 2 – an instantaneous temperature step, a constant heat flux and a wall temperature-time history that corresponds approximately to the Apollo 14 HFC boundary condition. Steady state convergence is obtained for boundary condition 1 and compared to an analytic steady solution. Results for boundary condition 3 are compared to a pure conduction analysis of the HFC configuration.

All of the results are shown in dimensionless units except HFC case 3 solutions which are given in dimensional form in the International System of Units.

4.2 PARALLEL PLATE MODEL

The first case considered uses the Model 1 equations with helium gas as the fluid. The gas is initially at rest with uniform temperature. At time t_o, the $x = 0$ surface is instantaneously raised to twice the initial temperature. The problem configuration and fluid properties are illustrated in Fig. 5. Larkin (Ref. 5) and Thuraisamy (Ref. 6) have also applied finite-difference calculations to this problem and comparisons to their solutions are made whenever possible.

The steady state solution to this problem can be obtained analytically. At steady state the fluid motion will vanish; thus we have

$$u_{ss} = 0 \tag{43}$$

where the subscript indicates a steady state value. The temperature profile should then approach the solution of the conduction equation with the prescribed boundary values. This solution is

$$T_{ss} = 2 - x \tag{44}$$

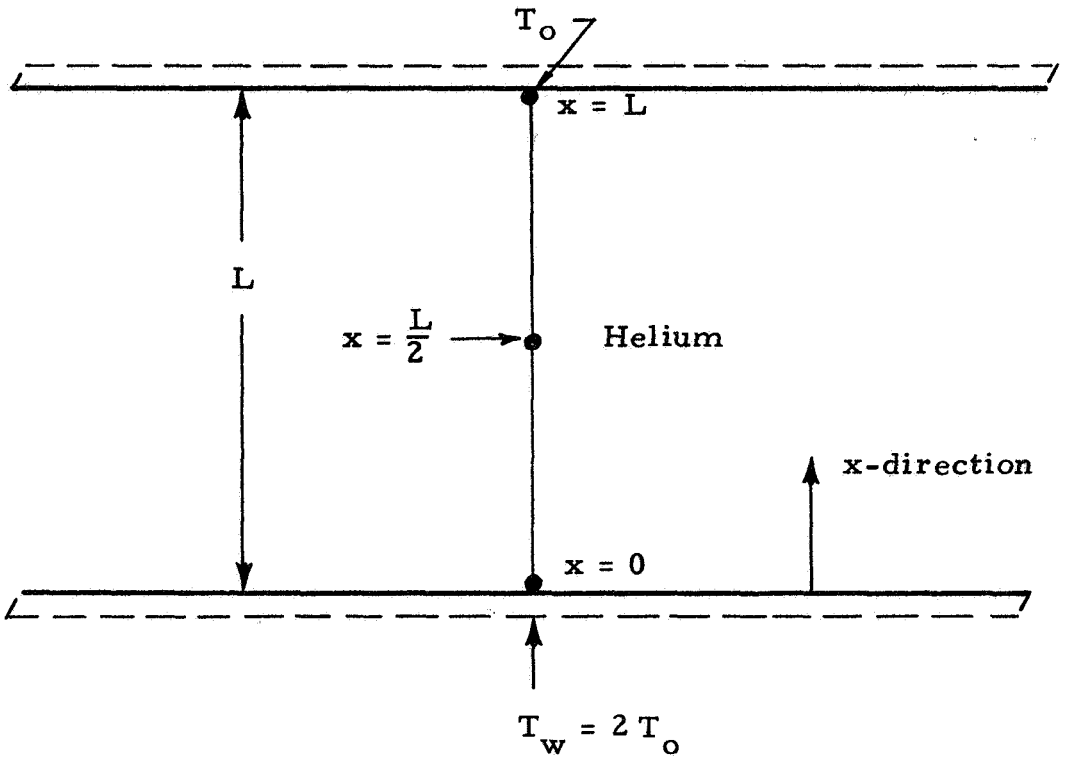

Properties of Helium

Property	Value
L	15.3 cm
ρ_o	1.9×10^{-4} gm/cm^3
P_o	1.01×10^{6} dyne/cm^2
T_o	273 ^oK
μ	1.875×10^{-4} gm/cm-sec
C_v	0.783 cal/gm-^oK
k	3.44×10^{-4} cal/cm-sec-^oK
γ	1.66
$\sqrt{RT_o}$	7.58×10^{4} cm/sec
T_w	$2T_o$

Fig. 5 - Configuration for Infinite Parallel Plate Model of Thermoacoustic Convection

From the momentum equation we then require

$$\left.\frac{\partial P}{\partial x}\right|_{ss} = 0 \text{ or } P_{ss} = \text{constant}$$

The value of this steady pressure can be found from the ideal gas equation of state by using the mass conservation condition that

$$\int_0^1 \rho dx = 1$$

We can integrate the $\rho = P/T$ profile to obtain

$$P_{ss} = \frac{1}{\ln 2} \simeq 1.44 \tag{45}$$

and

$$\rho_{ss} = \frac{1.44}{2 - x} \tag{46}$$

A scale factor $s = 1$ was used to calculate the transient solution to this problem to achieve an exact numerical simulation of the problem. The unsteady solution profiles are illustrated in Figs. 6-8. The sudden change in the wall temperature at $x = 0$ induces an expansion of the gas due to its compressibility. This expansion creates fluid motion in the $+x$ direction and the waves propagate to the $x = L$ surface and then reflect. The subsequent velocity field is then influenced by the reflections of this disturbance from each of the plates.

Figure 6 shows the calculated dimensionless velocity profile as a function of time for the first 400 time steps ($\Delta t = 0.025$). From this figure the oscillatory nature of the wave motion is seen. The period of the calculated waves is 1.55 units of dimensionless time. The acoustic wave period in this system of dimensionless units is $2/\sqrt{\gamma}$ and for helium is 1.55 units. The calculated waves are thus acoustic. This was also confirmed by Larkin's (Ref. 5) calculations. The maximum amplitude of these first few waves is approximately 0.02 units. Larkin's calculation yields an amplitude of approximately 0.2 units with a period of 1.55 units. The present calculation thus yields an order-of-magnitude lower

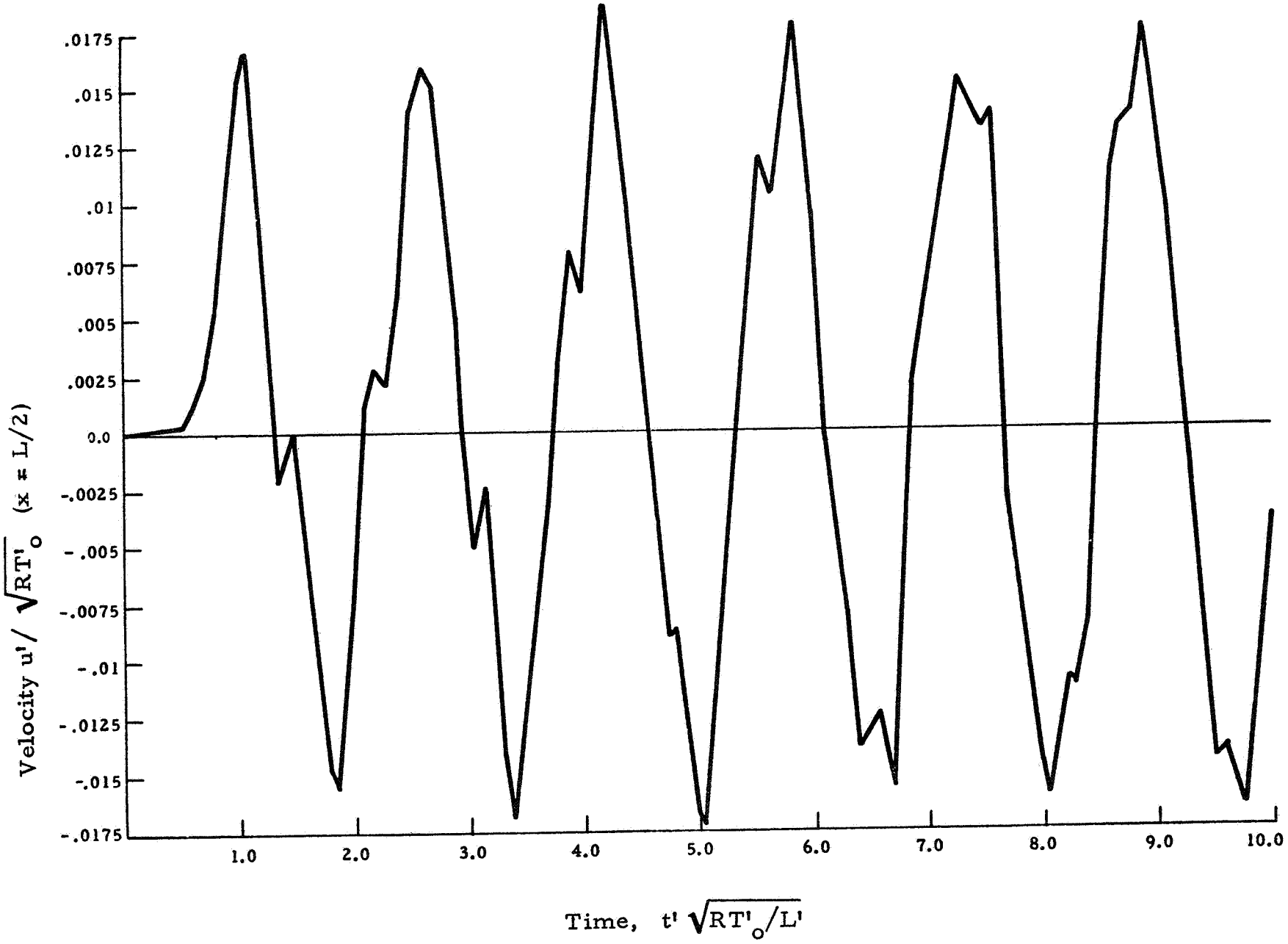

Fig. 6 — Velocity vs Time at Center Between Plates

amplitude than previously predicted. Thuraisamy (Ref. 6) used Larkin's numerical method to solve this problem and also calculated 0.2 for the amplitude.

Private communication with both Larkin and Thuraisamy and with S. W. Churchill of the University of Pennsylvania has resulted in the conclusion that the differences in the numerical method of Larkin and the present method are probably responsible for the noted discrepancies. The present calculation of 0.02 units appears to be more correct for the following reasons.

The quantity $u/\sqrt{RT_o}$ is a Mach number and would be expected to be "small" (relative to Mach 1) for natural convection flows. A Mach number of 0.02 appears to be more physically realistic for the present problems than 0.2. This is further confirmed by analyses on the similar problem of Sondhauss tubes by Feldman (Ref. 32) which indicated that the Mach number was always less than .06. To checkout this discrepancy further, a second order finite-difference method — The Dufort Frankel scheme — was developed at Lockheed independently of the present method. As discussed in Appendix B, this Dufort Frankel method also produced a calculation of approximately 0.02 for the wave amplitude. For these reasons the results of the present analysis shown in Fig. 6 are considered to be the true solution for the velocity profile.

The calculated temperature profile at t = 1000 units is shown in Fig. 7. The present calculation is in excellent agreement with those of Larkin and Thuraisamy. The solution at t = 1000 is seen to be much closer to the steady state than a conduction solution which neglects thermally induced fluid motion. This figure indicates that thermoacoustic convection is an effective transfer mechanism and greatly inhances the rate of heat transfer. It is interesting to note that the temperature profiles calculated by the present method are in excellent agreement with those of Larkin while the velocity amplitude calculations are quite different.

Figure 8 shows the calculated density profile and mean pressure distribution for this problem. The density distribution at t = 1000 has almost achieved its steady state profile. The spatially averaged pressure versus time is compared to Larkin's result. The agreement is excellent with only a slight discrepancy

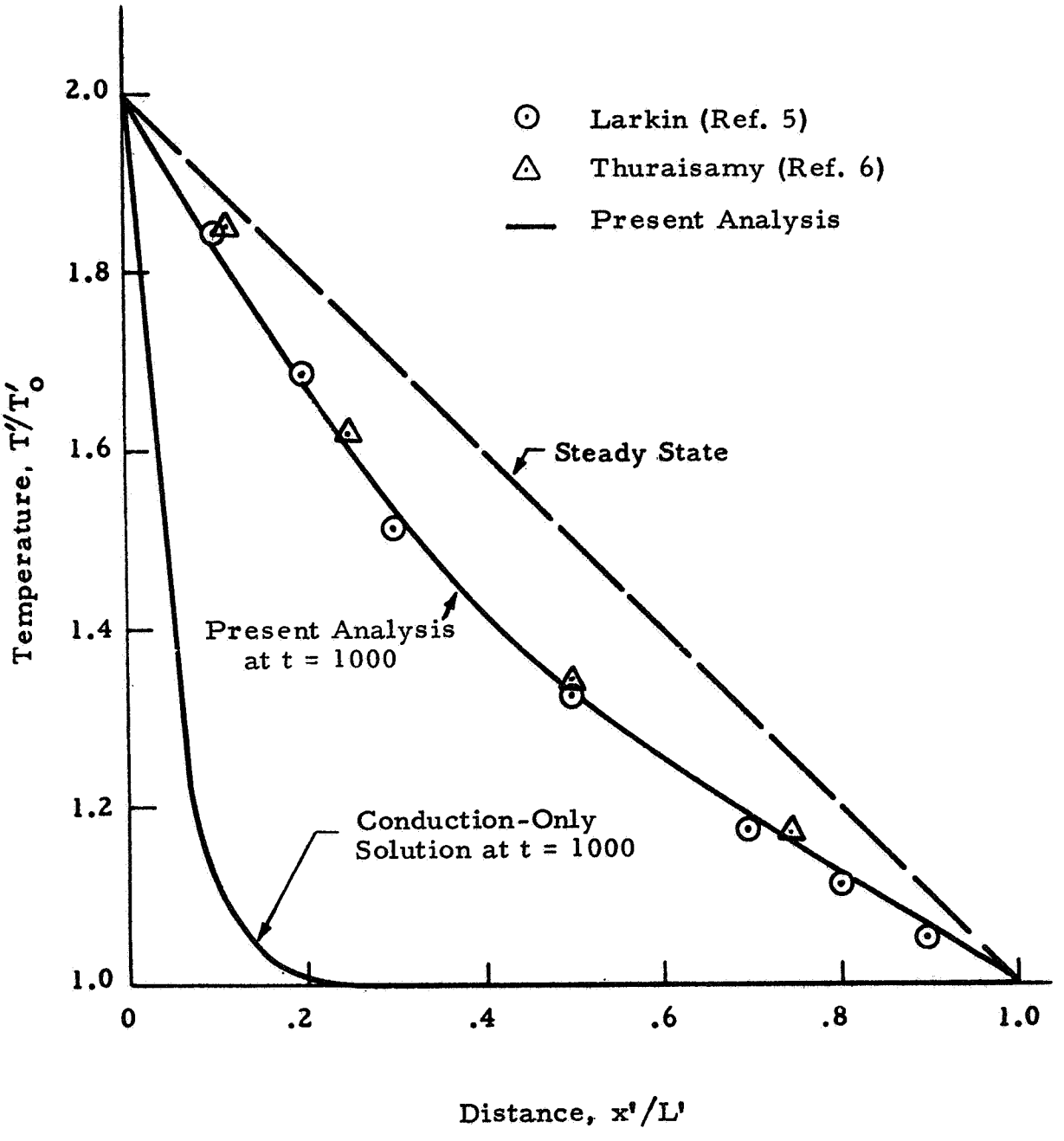

Fig. 7 — Temperature vs Distance at Time t' = 0.2 Seconds

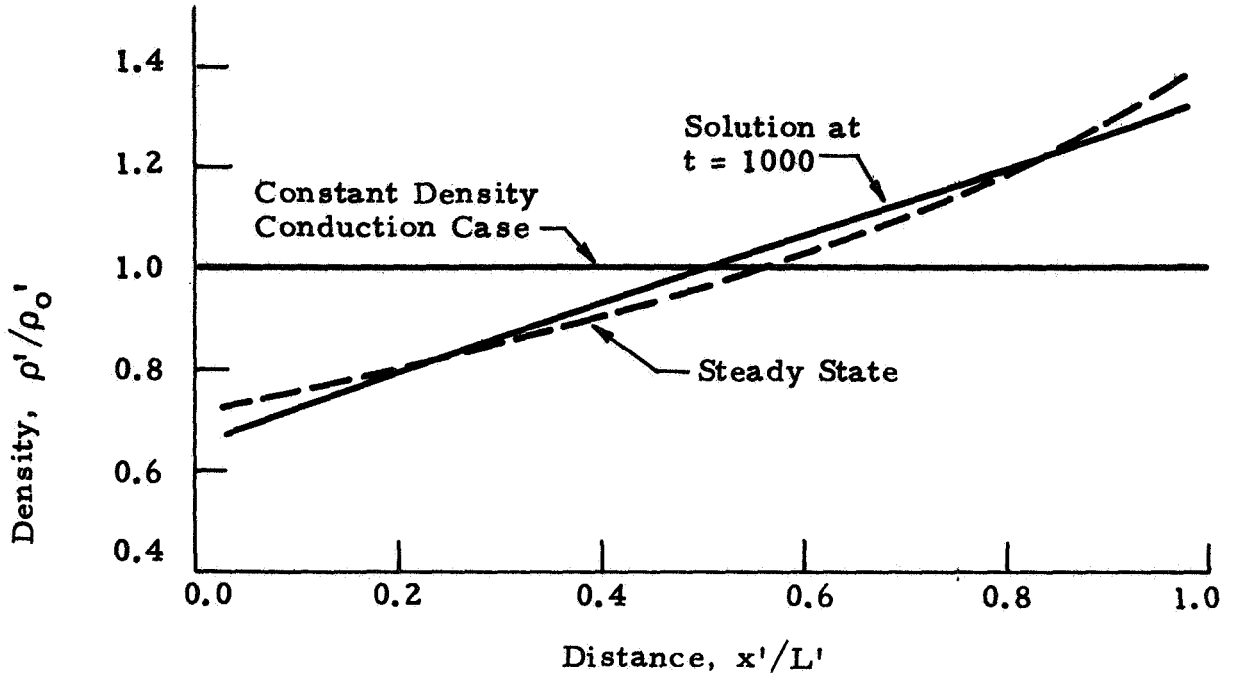

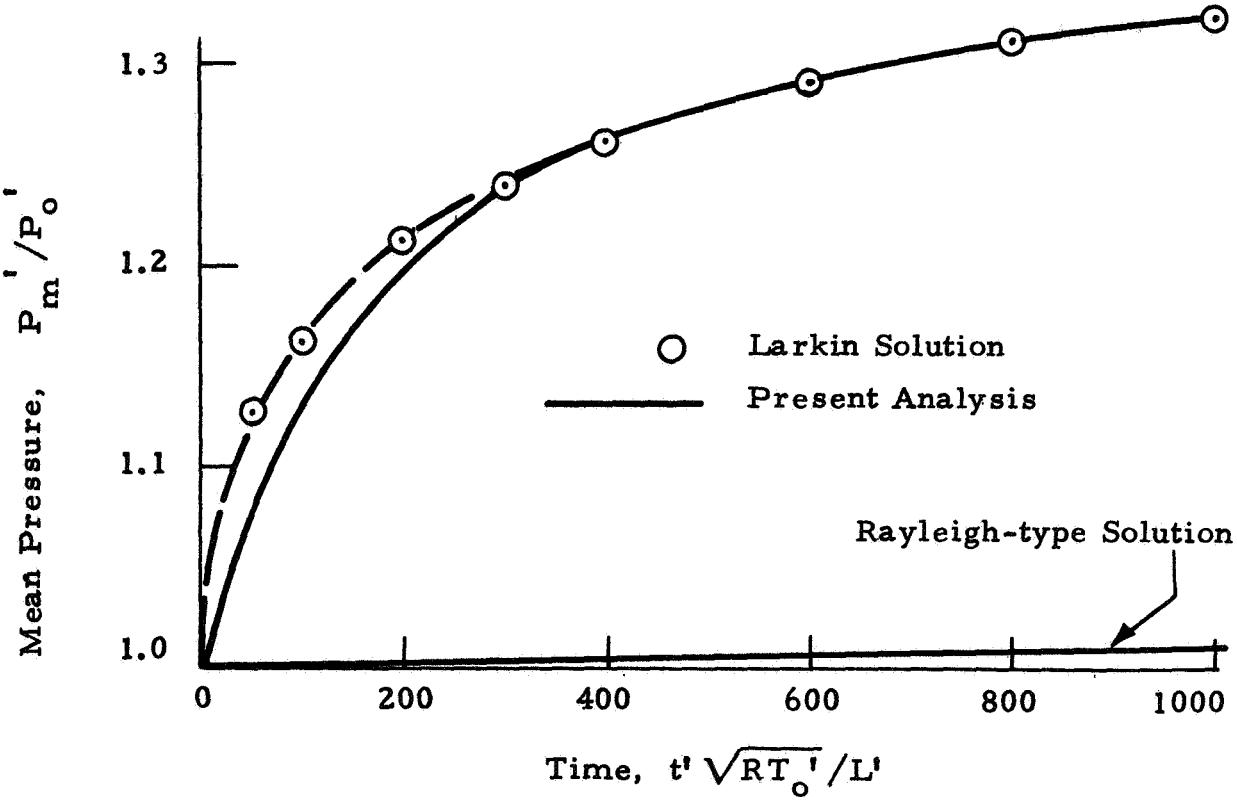

Fig. 8 - Density and Pressure Profiles for Infinite Plate Problem (Helium, $T_w = 2$)

at the early times. Note the large increase in pressure over that predicted by a Rayleigh-type solution. The Rayleigh solution is obtained by dropping all convective terms in the energy equation and computing mean pressure from the integral of the temperature profile with density constant, i.e. no convection. The strong influence of thermoacoustic convection on the rate of pressure rise is clearly seen. It is interesting to note that t = 1000 units corresponds to approximately 0.2 second of real time. The 30% rise in pressure in this short time may appear physically unrealistic, however, we should recall the severity of the thermal boundary condition ($T_w = 2T_o$). This result thus represents an upper limit on the rate of pressure rise due to thermoacoustic effects.

The calculations thus far have established that thermoacoustic convection can greatly enhance the rates of heat transfer and pressure rise. Reasonable agreement with previous solutions for the unsteady flow profiles has also been illustrated. To verify the steady state convergence of the method, the helium problem was solved with a scale factor s = 100 to achieve a "large" number of time step with a reasonable amount of computer time. With this scale factor, minute details of the unsteady profiles will be missed but the steady state should not be effected. Figure 9 illustrates the convergence of the computation. A plot of Nusselt number versus time shows that a steady state (Nu = 1) is approached. The definition of the unsteady Nusselt number used here is

$$Nu = \frac{\left.\frac{\partial T}{\partial x}\right|_w}{\Delta T_{ss}} \qquad (47)$$

where $\left.\frac{\partial T}{\partial x}\right|_w$ is the dimensionless temperature gradient at the heated wall ($x = 0$) and ΔT_{ss} is the steady state temperature difference $T_w - T_o$. The figure shows that the temperature profile near the x = 0 wall approaches its steady state in approximately 1000 units of time.

The mean pressure profile also smoothly approaches the true steady value of 1.44. Approximately 200,000 time steps or 50 seconds of real time

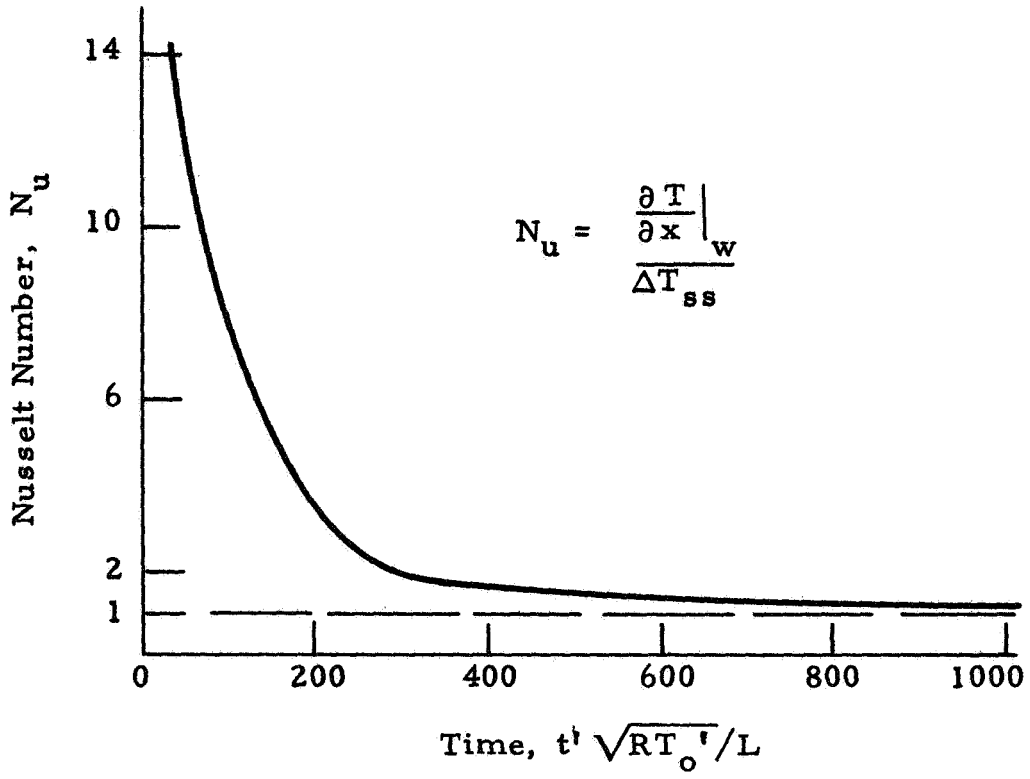

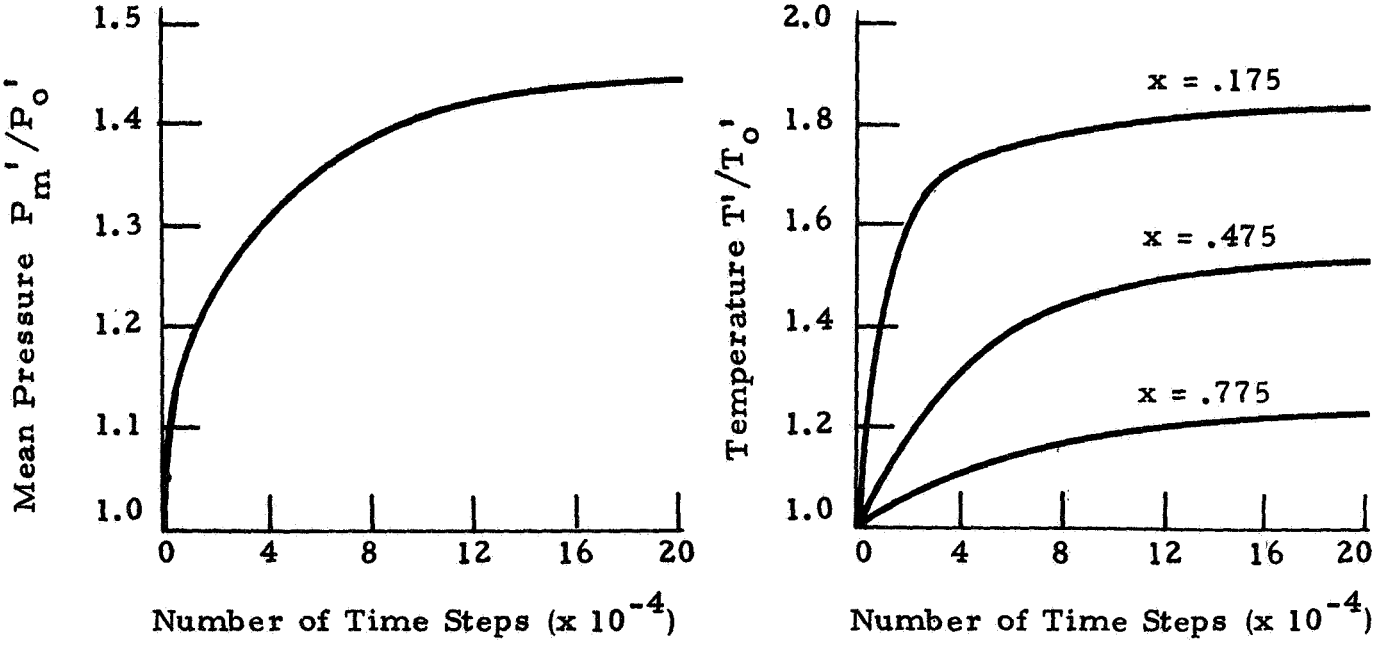

Fig. 9 - Illustration of Steady State Convergence of Numerical Method For Thermoacoustic Convection

was required to reach this constant steady state pressure. The spatial pressure distribution however remained constant after 80,000 steps, thus we have that

$$\frac{\partial P}{\partial x} \longrightarrow 0.$$

The velocity profile calculated after 80,000 steps showed a mean of $\sim 10^{-8}$ and after 200,000 steps was of the order of 10^{-12}, i.e. the wave motion is damped out as expected. Figure 9 also shows the unsteady temperature profiles for three locations in the flow. These also remain unchanged after about 200,000 calculation steps or 50 seconds.

The preceding calculations were carried out using 20 mesh points and a time of 0.025 units. The numerical solution of this problem for the unsteady profiles (Figs. 6, 7 and 8) required 3 minutes of computer CPU time on the Univac 1108 computer using a scale of s = 1 for exact simulation. The steady state convergence (200,000 time steps) using s = 100 required 15 minutes of CPU time. These computer time/real time ratios are not small but are well within the practical limits of the current state of the art. More sophisticated time-scaling methods could improve the computational economics even more.

Several interesting results were found concerning assumptions which are classically made in the numerical computation of natural convection. These were explored to determine the importance of viscous dissipation and pressure convection on the solutions of the energy equation. The viscous dissipation term in the energy equation is usually neglected in numerical solutions of natural convection. An order of magnitude analysis was performed and it appeared justifiable to neglect this term. To verify this assumption, the TC1 program was modified to include the dissipation term

$$\phi' = \mu' \left(\frac{\partial u'}{\partial x'}\right)^2 \qquad (48)$$

The infinite parallel plate problem was solved with ϕ included and compared to

the solution neglecting dissipation. Typical results at t = 1000 are shown below. This clearly verifies the relative unimportance of viscous dissipation even for a severe thermal boundary condition $T_w = 2$.

Quantity	Without ϕ	With ϕ
T (x = .025)	1.9603	1.9611
T (x = .975)	1.02175	1.01302
ρ (x= .025)	0.6749	0.6751
ρ (x= .975)	1.305	1.306
P_{avg}	1.3266	1.3261
Nu	1.286	1.254

Classical formulations of the thermal convection problem have utilized the Boussinesq approach which treats quasi-incompressible fluids as discussed in Section 2. Most studies which have considered compressible flows have not given full consideration to the effects of spatial pressure gradients on the flow work in the conservation of energy equation. A simple, yet informative study was made to determine the consequences of such an approximation on the unsteady flow profiles.

Consider the energy equation Eq. (7) written in terms of the constant pressure specific heat C_p. The flow work term for one dimensional geometry is then

$$\frac{\partial P}{\partial t} + u \frac{\partial P}{\partial x} . \qquad (49)$$

The present analysis to this point has included the full flow work term Eq. (49). For the purpose of evaluating the importance of the pressure convection term $u \frac{\partial P}{\partial x}$, the following modification was made.

- The $u \frac{\partial P}{\partial x}$ is assumed small and is neglected.
- $\frac{\partial P}{\partial t}$ is calculated from a spatial mean pressure and varies only with time.

This approach follows a classical method of analysis for natural convection. This case was solved using the helium parallel plate problem to compare the solutions with and without pressure convection.

Figure 10 shows profiles of pressure and temperature versus time with and without the $u\,\partial P/\partial x$ pressure convection term. It is evident from these curves that the term cannot be neglected for the sample problem studied. There is considerable deviation in the unsteady profiles for both temperature and pressure. It is interesting to note that the temperature is higher without the pressure term than with it. Neglect of $\partial P/\partial x$ implies that the pressure is constant across the region between the two plates. Since there is a thermal gradient across the fluid field, this implies that the pressure equalizes instantaneously; i.e., the pressure waves propagate at an infinite speed rather than at the true speed of sound. This is shown by Fig. 10 since this figure indicates that heat from the wall is being transferred to the fluid faster due to the infinite wave speed. Note that both the pressure and temperature profiles achieve their steady state much more rapidly if the finite wave speed is neglected.

For this sample problem we must conclude that neglect of pressure convection is not justified. Although no general conclusion can be made from this one case, we are alerted to the fact that the finite wave speed may be important in studying convection of fluids which are rapidly heated. A more detailed parametric study, with heating rate as the parameter, could be performed to determine the ranges of heating rate where this effect is important.

4.3 RADIAL MODEL

Computations are presented for a second configuration which uses the Model 2 equations with carbon dioxide as the fluid. This model represents a

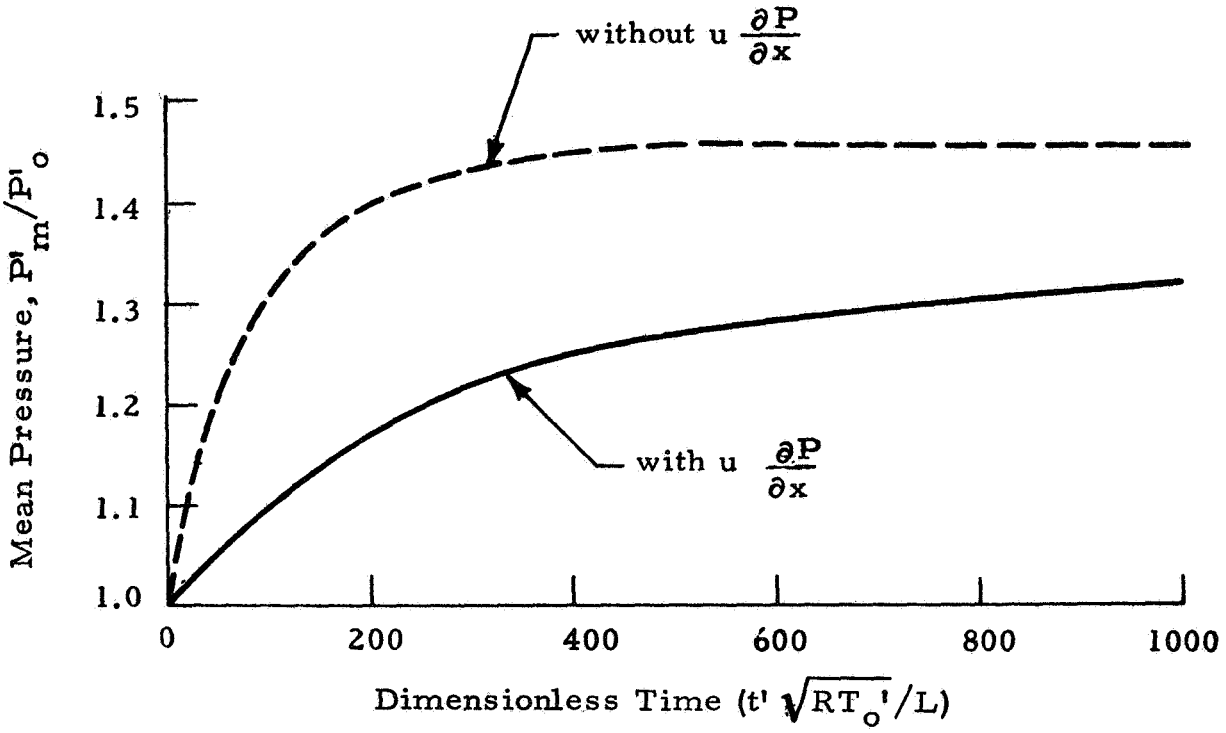

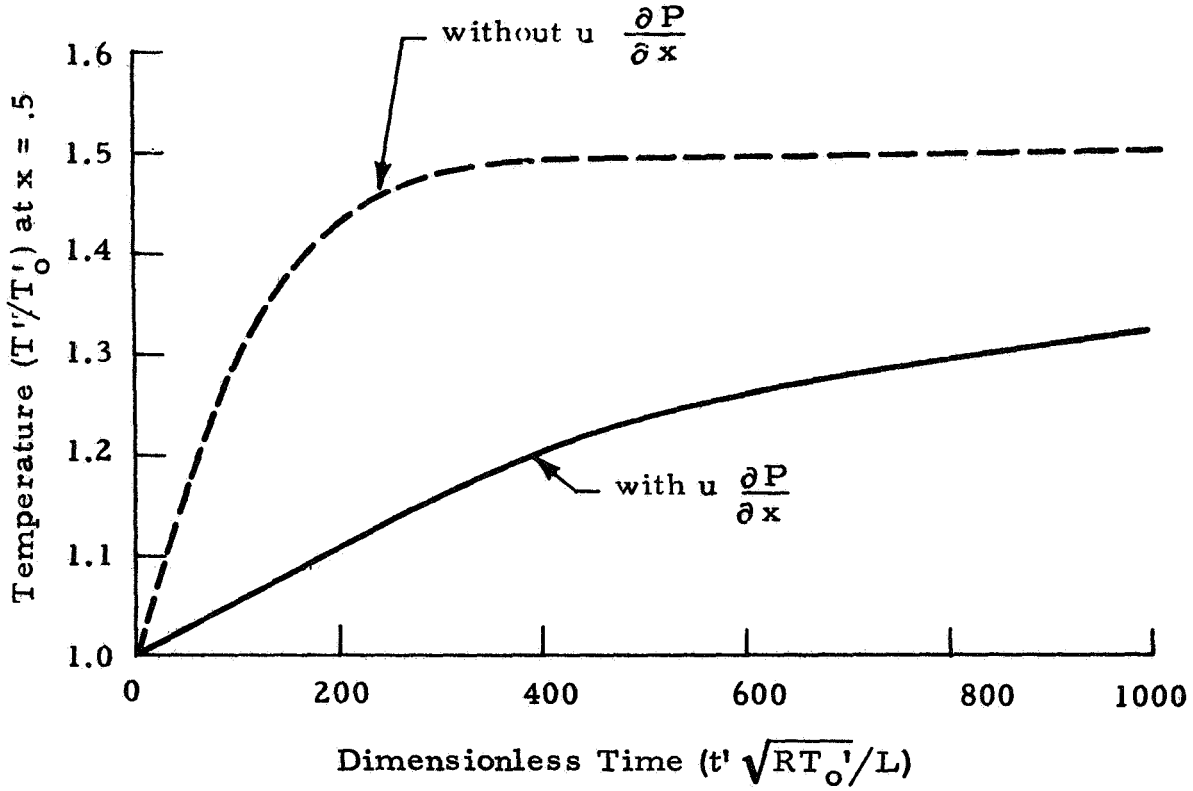

Fig. 10 - Pressure and Temperature vs Time Illustrating the Importance of Pressure Convection Term in Energy Equation

one-dimensional radial segment of the Apollo 14 Heat Flow and Convection Demonstration (Ref. 1) radial cell experiment. The HFC radial cell, the one-dimensional mathematical model, and a list of fluid properties used, is given in Fig. 11. Three types of thermal boundary conditions are applied to this configuration:

- Instantaneous wall temperature step

  $T_w' = 2T_o'$,

- Constant heat flux

  q_w' = constant

- Wall temperature-time history prescribed

  $T_w' = f'(t')$

These are boundary conditions on the $r = r_o$ surface, i.e., the inner cylinder which is a heater. The outer wall is held isothermal except in the constant heat flux case where an adiabatic outer wall is assumed. The steady state solution for this model using the $T_w' = T_o'$ boundary condition can be easily established analytically but not for the other boundary values. As with Model 1, the "one-dimensional" motion will vanish at steady state, thus

$$u_{ss} = 0 \tag{50}$$

where the subscript indicates a steady state value. The temperature profile will then approach the solution of the conduction equation with the prescribed boundary conditions. This solution is

$$T_{ss} = \frac{\ln(r_o r)}{\ln r_o} \tag{51}$$

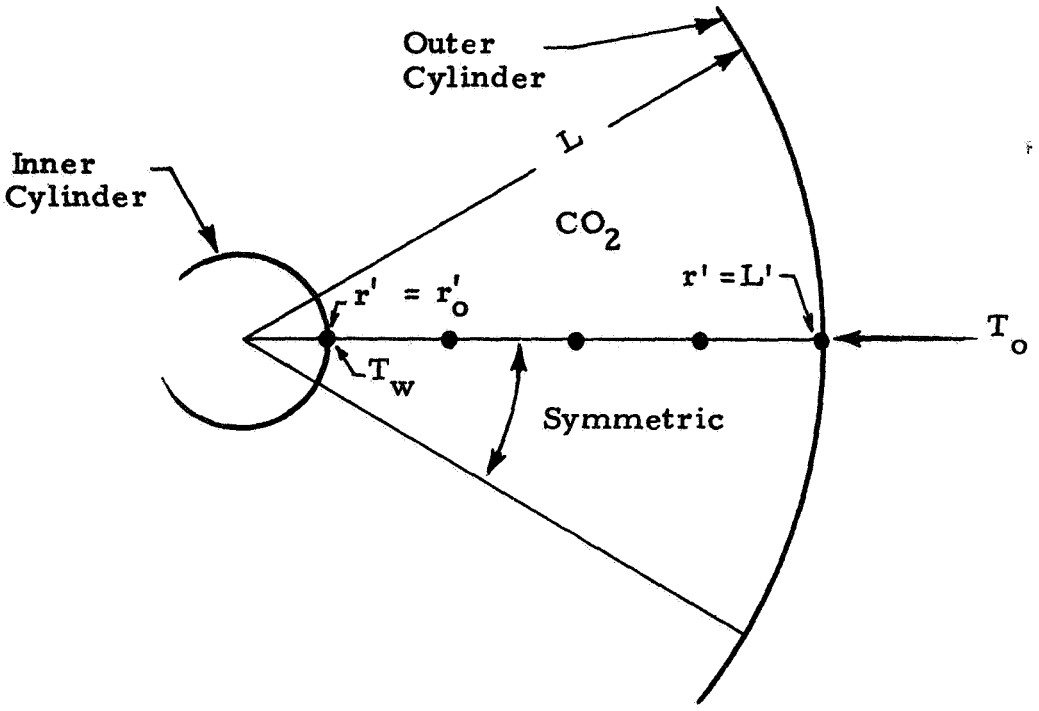

One-Dimensional Radial Model of HFC

Properties of CO_2	
Property	Value
L	3.175 cm
r_o	0.223 cm
ρ_o	1.6×10^{-3} gm/cm^3
P_o	1.013×10^{6} dyne/cm^2
T_o	296 ^oK
μ	1.70×10^{-4} gm/cm-sec
C_v	0.18 cal/gm-^oK
k	4.63×10^{-5} cal/cm-sec-^oK
γ	1.3
$\sqrt{RT_o}$	2.38×10^{4} cm/sec

Fig. 11 - Configuration for Cylinder Model of Thermoacoustic Convection

From the momentum equation, we then require

$$\left.\frac{\partial P}{\partial r}\right|_{ss} = 0 \quad \text{or} \quad P_{ss} = \text{constant}$$

The value of this steady pressure can be found from the ideal gas equation of state by using the mass conservation condition that

$$\int_{r_o}^{1} r\rho dr = \frac{1 - r_o^2}{2}$$

We can integrate the $\rho = \frac{P}{T}$ profile to obtain an infinite series for the steady steady state pressure. Taking r_o as in Fig. 11, we get

$$P_{ss} \approx 1.16 \tag{52}$$

and

$$\rho_{ss} = \frac{1.16 \ln r_o}{\ln (r_o r)} \tag{53}$$

A scale factor $s = 1$ was used for the case $T_w = 2T_o$ to examine the exact nature of the wave motion and profiles for the cylindrical model. The unsteady flow profiles for this case are given in Figs. 12 through 14. The oscillatory velocity profile shown in Fig. 12 is similar to that produced for the parallel plate model (Fig. 6). The period of the acoustic waves is 1.62 with a maximum amplitude of 0.03 units. The wave amplitude is slightly higher than the plate model and the waves themselves appear more "irregular" than those in Fig. 6. The amplitude is still of the order of 0.02 and not 0.2 as discussed in Section 4.2.

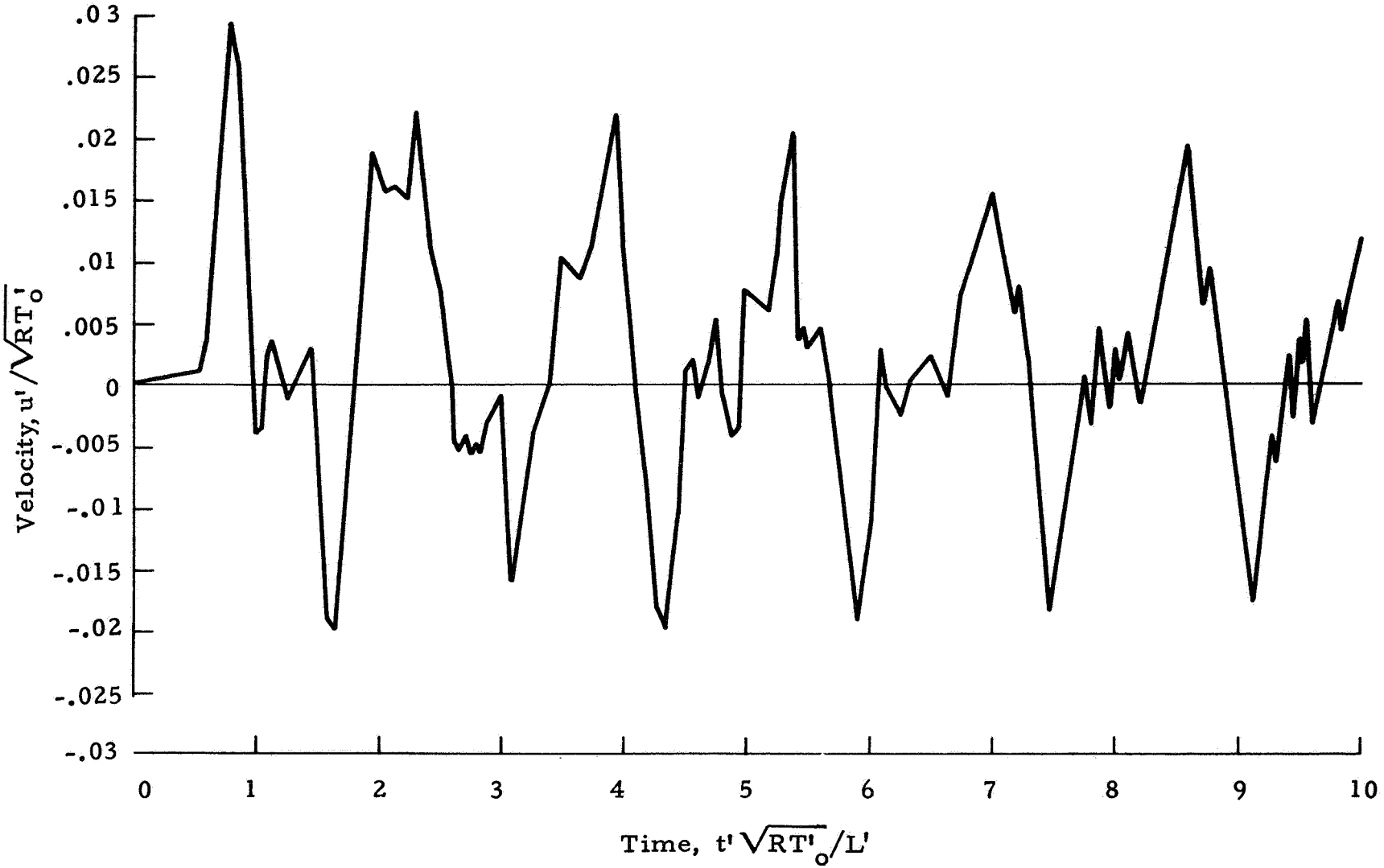

Fig. 12 — Velocity vs Time at r = .571 for Radial Model (T_w = 2)

Figure 13 gives temperature, pressure and density profiles for the $T_w' = 2T_o'$ case. The calculated temperature profile versus radial distance at t = 350 units again indicates the large increase in heat transfer compared to a conduction only model. The thermoacoustic effect is also an important heat transfer mechanism for the radial configuration. The solution profile is seen to be approaching a true steady state condition which it achieves near t = 1000 units. The spatial mean pressure rise versus time is again considerably above that of a conduction (Rayleigh-type) solution but is not as drastic a rise as given by the plate model (Fig. 8). The density profile is shown as a function of radial distance at t = 1000 and indicates the smoothness of the steady state profile. These calculations are in excellent agreement with the analytical steady state given by Eqs. (50) through (53.).

Figure 14 shows the spatial velocity distribution for t = 10 and t = 500. The smoothness of the profiles versus r indicates that the numerical method is very satisfactory for calculating the relatively slow flow of natural convection. This case was also run for a scale s = 100 and profiles were calculated to t = 100,000. The damping out of the velocity profile gives good indication of the convergence of the numerical method. The velocity continued to damp out with time to a value about 10^{-14}. The temperature, pressure and density profiles at t = 100,000, or about 2 seconds, agreé with the analytical steady state to less than 0.1% deviation.

The computation time for this case was 3 minutes on the Univac 1108 Exec 8 using 20 mesh points and a time step $\Delta t = .025$.

The next case for the radial configuration consists of applying a constant heat flux boundary condition to the $r = r_o$ surface. A dimensionless heat input

$$q = \frac{q'L'}{k'T_o'} = 20 \qquad (54)$$

was used as the boundary value. When applied to the surface area of the inner

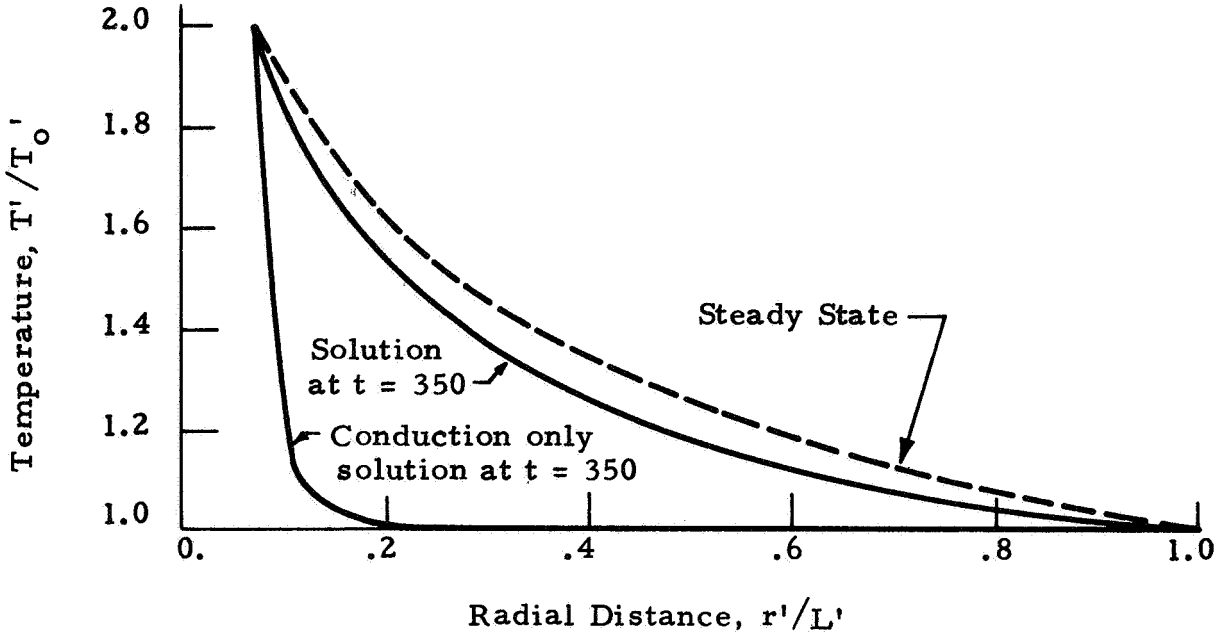

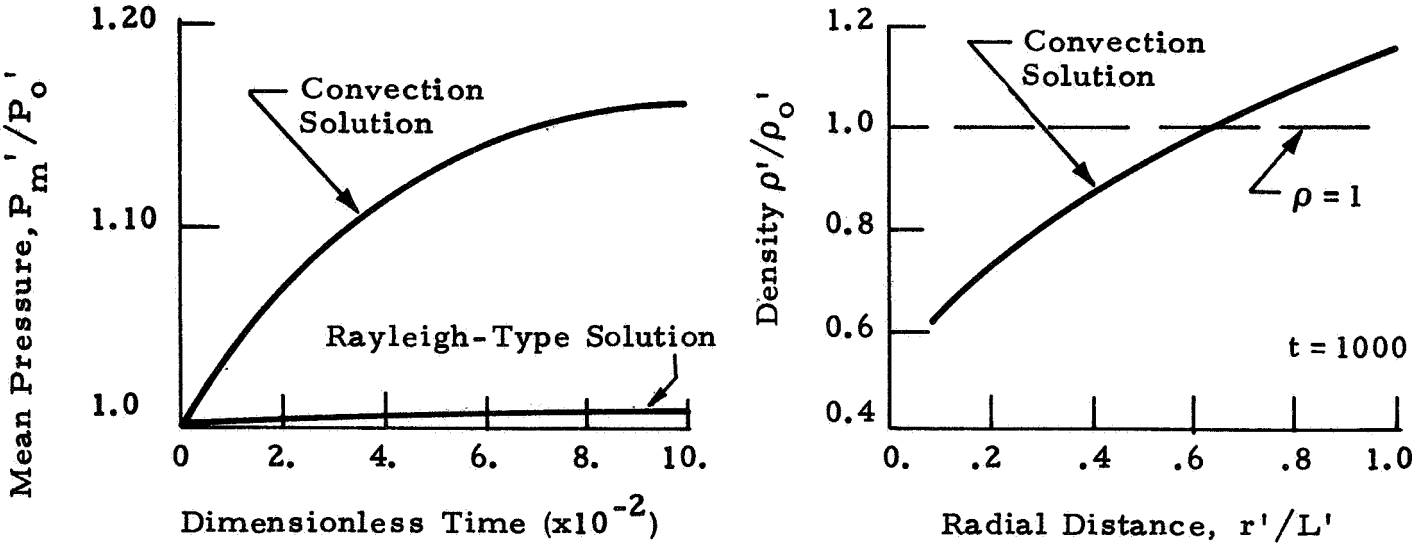

Fig. 13 - Temperature, Pressure and Density Profiles for Radial Model Problem ($T_w = 2$)

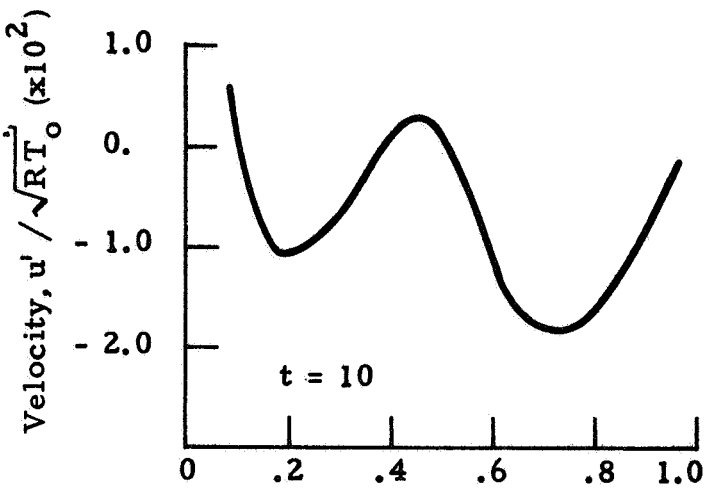

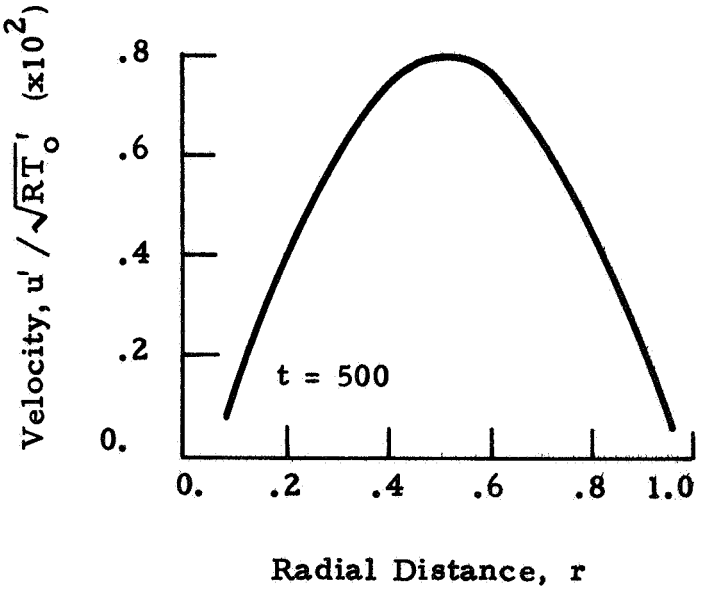

Fig. 14 - Velocity vs Radial Distance r for Two Time Points (Radial Problem $T_w = 2$)

cylinder, this corresponds to a heat input of 5.7 watts which is the heater power used to drive the HFC radial cell experiment. The r = 1 surface was considered adiabatic for this case.

A scale factor s = 1 was used to calculate the unsteady flow profiles to t = 2000 units. The velocity waves and pressure rise for this constant heat flux case were much less severe than the $T_w' = 2T_o'$ boundary condition. However, the unsteady temperature profiles for fluid points near the heated surface exhibit an interesting behavior as illustrated in Fig. 15. The convection solution is compared to a conduction only solution at $r = r_o$ (at the heated surface) and r = 0.093 (near the heated surface). At the early times, the fluid at and near the heated wall gets hotter than by pure conduction indicating an effective fluid convective mechanism. At about t = 1200 the conduction solution has "caught-up" and the local temperature calculated by conduction alone at these r-locations continue to rise with time. The convection solution, however, tends to steady out with time at these same r-locations since the convection mechanism is now transfering the incoming heat to further portions of the fluid. This same behavior was exhibited at locations further from the wall at later times. Although no direct comparison with flight data is possible for this case, the behavior is qualitatively the same as that obtained in the HFC flight experiment, Fig. 1. Computation time was six minutes.

A third type of boundary condition was applied to the radial configuration. This boundary condition consists of a profile of the $r = r_o$ wall temperature as a function of time. The computer program was modified to perform a table look-up and interpolation at each time step to obtain the psuedo-constant wall temperature. The profile that was used was obtained from a detailed conduction network analysis of the actual HFC radial cell experiment. An inhouse Lockheed thermal analysis program (Ref. 31) was used to calculate temperatures at 100 points in the HFC radial cell including the inner cylinder heater post. This heater post temperature profile was then used as an input boundary condition to the radial model convection program. The outer wall temperature history as calculated by the conduction network showed this surface to be essentially isothermal. These boundary conditions are shown graphically in the top curve of Fig. 16.

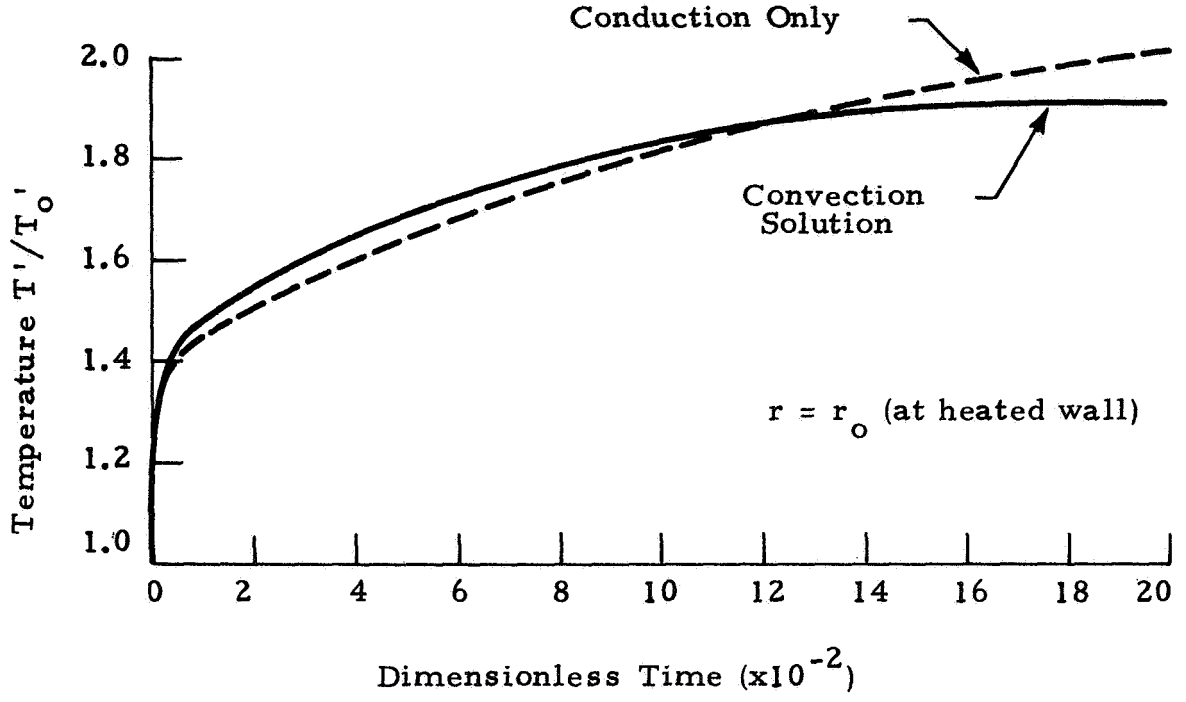

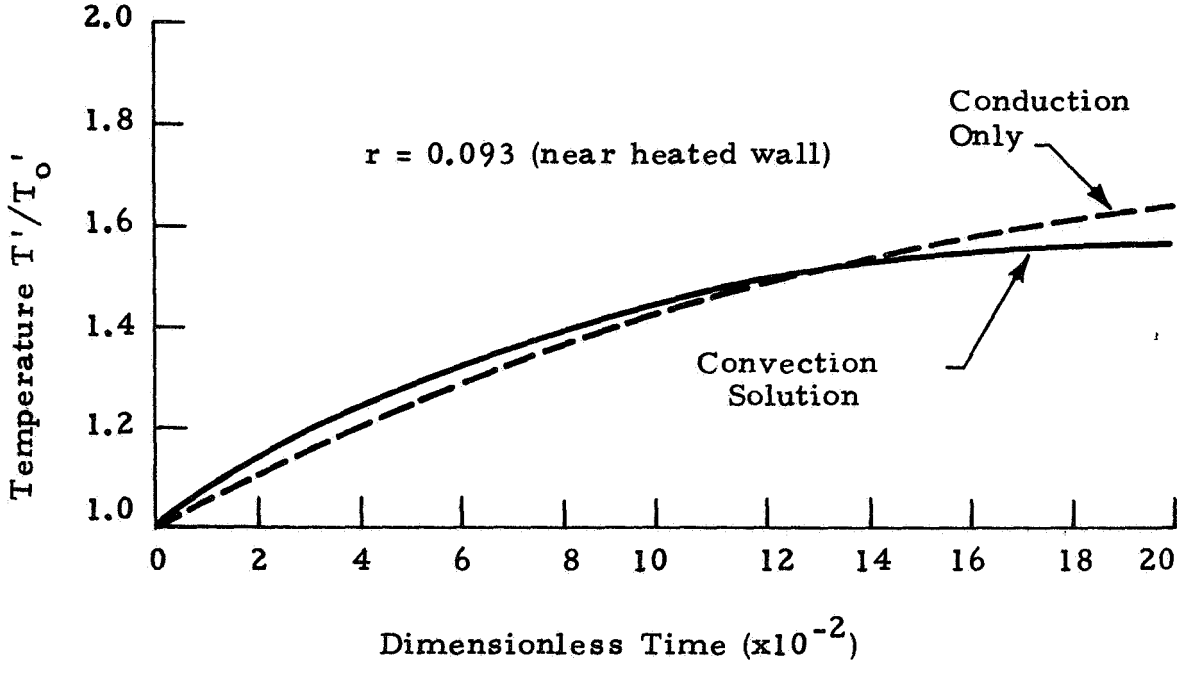

Fig. 15 - Temperature vs Time at Two Radial Locations Comparing Solutions to Conduction-Only Results (q_w = 20 Boundary Condition)

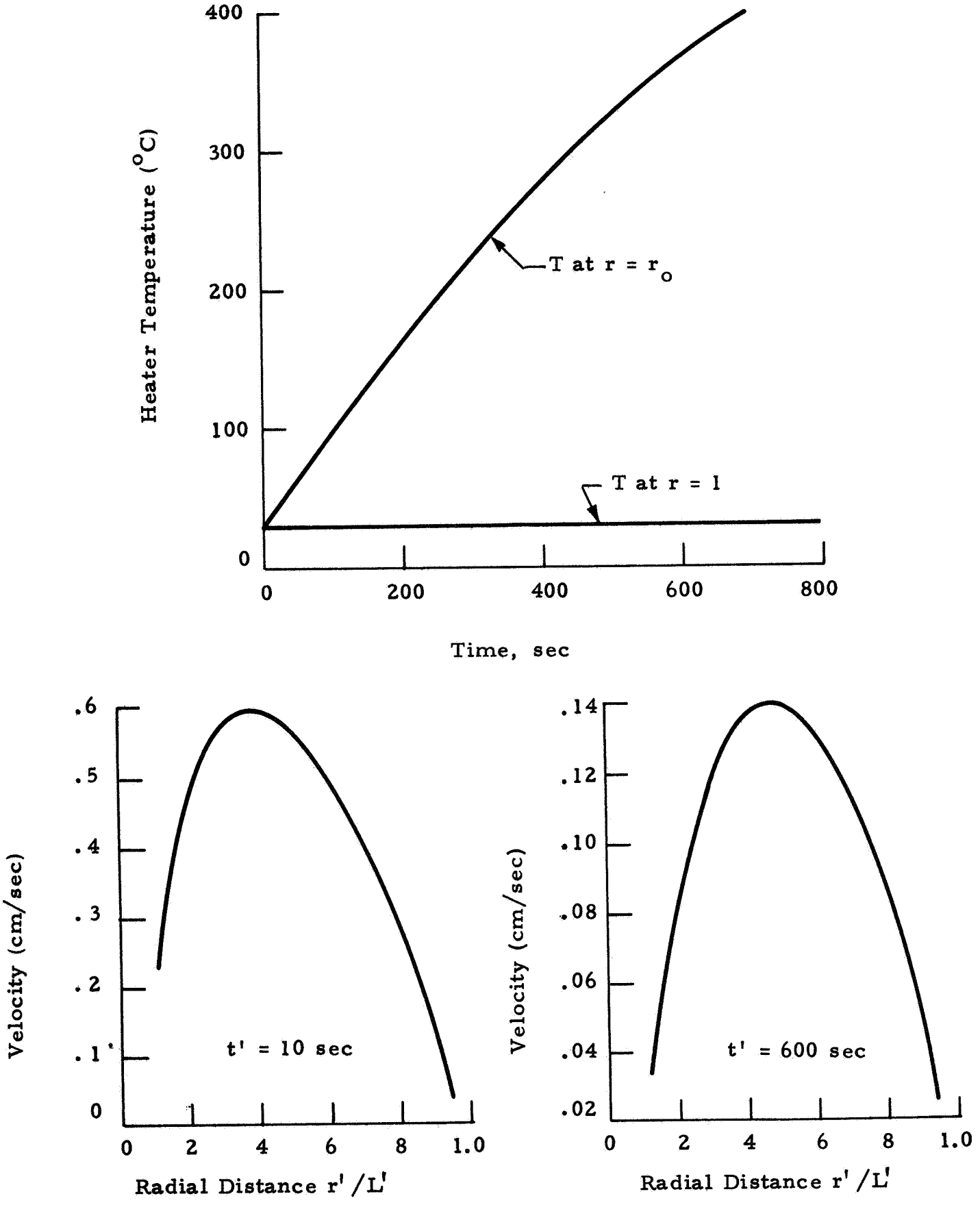

Fig. 16 - Heater Temperature and Velocity Profiles for Apollo 14 HFC Radial Simulation (T_w vs t Boundary Condition)

A complete analysis of the HFC requires that 600 seconds of real time be simulated. For this reason a scale factor s = 100 was used for the calculation of this model. This time scaling should yield a quiet accurate simulation due to the relatively slow heater temperature rise. Figure 16 shows the calculated spatial velocity distribution at t = 10 seconds and t = 600 seconds. At the early times, flow velocities of the order of 0.5 cm/sec are calculated. As the simulation time increases these velocities are damped out to values the order of 0.1 cm/sec at t = 600 seconds. It is interesting to note that the peak velocities occur at r'/L' = 0.4 to 0.5, i.e., near the center of the radial segment. This same behavior was exhibited at the intermediate time points also. The velocity wave motion for this case was much more highly damped than those obtained using the severe $T_w' = 2T_o'$ condition.

Figure 17 gives profiles of the calculated temperature versus time at radial locations r' = .69 cm and r' = 1.65 cm. It should be noted at the outset that no flight data are shown on this figure for the following reason. The Apollo 14 HFC radial cell experiment uses liquid crystal temperature indicators which must be placed in view of a Data Acquisition Camera. This prohibited the acquisition of data in the CO_2 gas at radial locations from the heater post. The one-dimensional radial convection model discussed here is used to obtain qualitative information related to the actual HFC demonstration. A two-dimensional analysis, discussed in Section 5, is needed in order to make comparisons to actual flight data.

However, Fig. 17 does show a very familiar behavior. The calculated temperatures are compared to a one-dimensional (radial) conduction only solution using the same numerical method for the energy equation as used for the convection analysis. Also shown for comparison are the results of the detailed two-dimensional (axisymmetric) conduction network analysis using the Lockheed conduction program (Ref. 31). At both the radial locations shown the convection solution profile rises higher initially than pure conduction and then "flattens" out. At t = 600 seconds, the temperatures are lower than those predicted by pure conduction.

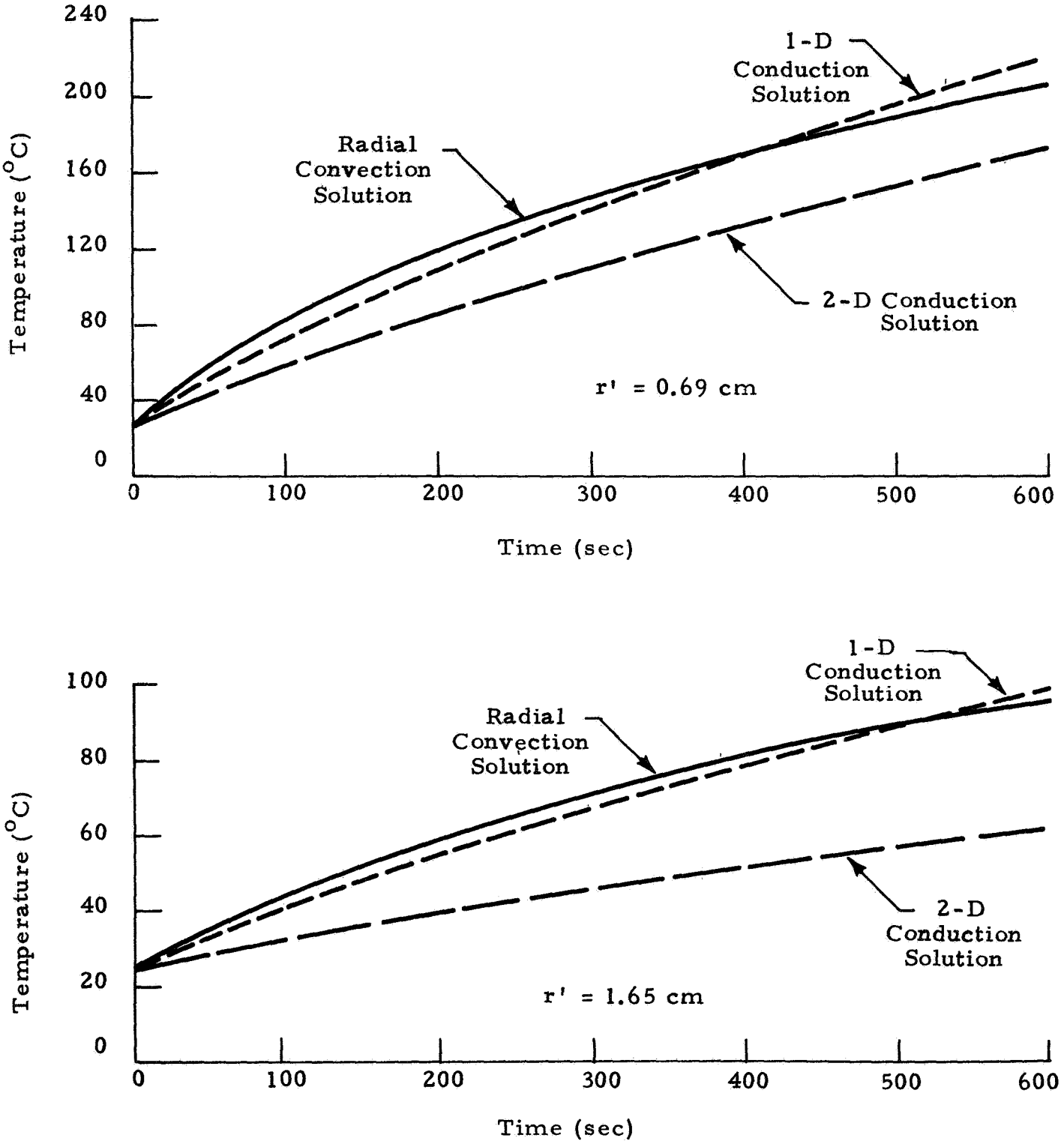

Fig. 17 - Temperature vs Time for Two Radial Locations in Apollo 14 HFC Radial Cell Simulation (T_w vs τ Boundary Condition)

This is the type of behavior exhibited by the flight data comparison given in Fig. 1 and discussed in Ref. 1. The magnitudes of the temperature differences shown in Fig. 17 are not as large as the HFC flight data analysis of Ref. 1 predicts. The largest difference in Fig. 17 is the order of 5% between convection and pure conduction. It is interesting to note the large deviation between the one-dimensional and two-dimensional conduction solutions. This suggests that multi-dimensional convection may also be important in determining the proper magnitude of the temperatures for this configuration. It is also emphasized that gravity convection was not included in the solutions shown in Fig. 17. The effects of gravity-driven convection would produce a larger deviation between the conduction and convection solutions of Fig. 17. Gravity convection plus thermoacoustic effects could possibly explain the behavior of the Apollo 14 HFC data.

The results of this model, displayed in Fig. 17, leads us to the following conclusions·

- Thermoacoustic convection effects can qualitatively cause the type of behavior seen in the Apollo 14 HFC radial cell experiment
- The magnitude of the temperature differences between convection profiles and conduction-only profiles are not as large as indicated by the flight data analysis of Fig. 1
- Multi-dimensional convection effects may be important for the HFC configuration and
- The coupling of gravity-convection with thermoacoustic effects could possibly explain the behavior of the HFC flight data.

Section 5
CONCLUSIONS AND RECOMMENDATIONS

5.1 CONCLUSIONS

Several conclusions are evident from this numerical study of thermoacoustic convection in low gravity. These are summarized below in two categories — thermoacoustic effects and the numerical method.

5.1.1 Thermoacoustic Effects

The sample calculations presented in Section 4 have shown that thermoacoustic convection can be an important heat transfer mechanism. Specifically, it was shown that:

- The thermally induced wave motion is acoustical.
- Thermoacoustic convection can greatly enhance the rate of heat transfer.
- The mean pressure rise in a confined fluid is more rapid due to thermoacoustic effects.
- Pressure convection effects on the conservation of energy can strongly influence the transient fluid behavior.
- The magnitude of the effects of thermoacoustic convection is a strong function of the severity of the thermal boundary conditions.
- Thermoacoustic convection can cause flow phenomena similar to that observed in the Apollo 14 HFC flight demonstration.
- Quantitative comparison of theory to flight data will require a multi-dimensional analysis of thermoacoustic convection.

The general conclusion is summarized as follows: For low-gravity space processing situations involving confined compressible fluids which are heated, the thermally induced fluid motion should not be neglected in performing analytical design studies.

5.1.2 Numerical Method

The numerical calculation method used in this study has proved to be very satisfactory for computation of natural convection flows. It has been shown that the method:

- Is conditionally stable with the hyperbolic limit restricting the time step size.
- Is sufficiently accurate for space processing applications.
- Converges to an accurate steady state for the problems studied.
- Is computationally economic by state-of-the-art standards.
- Is readily adaptable to time scaling laws to reduce the computer time/real time ratio.
- Should be applicable to multidimensional natural convection computation.
- Can be readily adapted to the computation of other types of convection such as gravity driven or surface tension driven flows.

The numerical computation technique derived in this study has a wide variety of applications in the analysis of convection in space manufacturing processes.

5.2 RECOMMENDATIONS

Recommendations resulting from this study are offered for further investigation of thermoacoustic convection for space processing applications. It is recommended that the future effort consist of two tasks conducted in parallel.

Task 1. Develop a two-dimensional/axisymmetric computer program for analysis of thermal convection of compressible fluids.

Task 2. Conduct a simple ground-based laboratory experiment to investigate thermoacoustic convection in confined fluids.

The two-dimensional program should include, as a minimum, gravity driven convection and thermoacoustic convection. The direction of the gravity

vector with respect to the heated surface should be arbitrary. Both rectangular and cylindrical geometries should be included as options. The proven numerical method used for this one-dimensional study can be extended for use in the two-dimensional program. This capability will allow the coupling effects of gravity and thermoacoustic waves to be analyzed. The program will also provide a base for further extension to analyze convection in space manufacturing processes such as crystal growth, melting and/or casting of metals and chemical separation processes.

The experimental program should be kept relatively simple while retaining enough sophistication to obtain quantitative data. The experimental apparatus should primarily consist of a container of gas, a heater capable of rapidly raising the gas temperature, a system of sensitive pressure transducers, thermocouples, and recording instrumentation. The primary purpose should be to detect the pressure waves in order to study their amplitude, to measure gas temperatures for comparison with theory and to investigate the coupling of gravity to thermoacoustic effects.

This parallel effort will provide additional insight into the thermoacoustic phenomena, provide experimental data for comparison with theory, and will provide a basic convection computer program for analysis of future space manufacturing systems.

Section 6
REFERENCES

1. Grodzka, P. G., C. Fan, and R. O. Hedden, "The Apollo 14 Heat Flow and Convection Demonstration Experiments," LMSC-HREC D225333, Lockheed Missiles & Space Company, Huntsville, Ala., September 1971.

2. Trilling, L., "On Thermally Induced Sound Fields," J. Acoustical Soc. Am., Vol. 27, 1955.

3. Knudsen, J. R., "The Effects of Viscosity and Heat Conductivity on the Transmission of Plane Sound Waves," J. Acoustical Soc. Am., Vol. 26, 1957.

4. Luikov, A. V, and B. M. Berkoresky, "Thermoconvective Waves," Int. J. Heat Mass Trans., Vol. 13, 1970.

5. Larkin, B. K., "Heat Flow to a Confined Fluid in Zero Gravity," Progress in Astronautics and Aeronautics, Thermophysics of Spacecraft and Planetary Bodies, ed. by G. B. Heller, Vol. 20, 1967.

6. Thuraisamy, V., "Thermodynamic Flow of Super-Critical Oxygen in Zero-Gravity," Bellcomm TM-72-1022-1, Bellcomm, Inc., Washington, D. C., March 1972.

7. Aris, R., Vectors, Tensors, and the Basic Equations of Fluid Mechanics, Prentice-Hall, New, Jersey, 1962.

8. Eskinazi, S., Vector Mechanics of Fluids and Magnetofluids, Academic Press, New York, 1967.

9. Cheng, S. I., "Numerical Integration of Navier-Stokes Equation," AIAA J., Vol. 8, No. 12, December 1970.

10. Ostrach, Simon, "Role of Analysis in Solution of Complex Physical Problems," Invited Lecture, 3rd International Heat Transfer Conference, August 1966.

11. Hellums, J. D., and S. W. Churchill, "Dimensional Analysis and Natural Convection," Chemical Engineering Progress Symposium Series, No. 32, Vol. 57.

12. Hellums, J. D., and S. W. Churchill, "Computation of Natural Convection by Finite Difference Methods," Intl. Developments Heat Trans., Part I, Amer. Soc., Mech. Eng., New York, 1971.

13. Hellums, J. D., and S. W. Churchill, "Transient and Steady State, Free and Natural Convection, Numerical Solutions," AIChE J., Vol. 8, No. 5, November 1962.

14. Fromm, J. E., "Numerical Solutions of the Nonlinear Equations for a Heated Fluid Layer," Phys. Fluids, Vol. 8, No. 10, October, 1965.

15. Clark, J. A., and H. Z. Barakat, "Transient, Laminar, Free-Convection Heat and Mass Transfer in Closed, Partially Filled, Liquid Containers," ORA 04268, University of Michigan, Ann Arbor, 1965.

16. Wilkes, J. O., and S. W. Churchill, "The Finite Difference Computation of Natural Convection in a Rectangular Enclosure," AIChE J., Vol. 12, No. 1, January 1966.

17. Larkin, B. K., "Numerical Solution of the Continuity Equation," AIChE J., Vol. 12, No. 5, November 1966.

18. Samuels, M. R., and S. W. Churchill, "Stability of a Fluid in a Rectangular Region Heated from Below," AIChE J., Vol. 13, No. 1, January 1967.

19. Aziz, K., and J. D. Hellums, "Numerical Solution of the Three-Dimensional Equations of Motion for Laminar Natural Convection," Phys. Fluids, Vol. 10, No. 2, February 1967.

20. Torrance, K. E., "Comparison of Finite-Difference Computations of Natural Convection," J. Research, National Bureau of Standards, Vol. 72B, No. 4., October 1968.

21. Plows, W. H., "Some Numerical Results for Two-Dimensional Steady Laminar Bénard Convection," Phys. Fluids, Vol. 11, No. 8, August 1968.

22. Schwab, T. H., and K. J. DeWitt, "Numerical Investigation of Free Convection between Two Vertical Coaxial Cylinders," AIChE J., Vol. 16, No. 6, November 1970.

23. Cabelli, A., and G. DeVahl Davis, "Numerical Study of the Bénard Cell," J. Fluid Mech., Vol. 45, Part. 4, 1971.

24. Heinmiller, P. J., "A Numerical Solution for the Prediction of Pressure Collapse in Supercritical Oxygen," TRW 17618-H080-R0-00, TRW System Group, Houston, Texas, 1970.

25. Barton, J. E. et al., "Apollo Oxygen Tank Stratification Analysis," Boeing D2-118407-1, Boeing Company, Houston, Texas, 1971.

26. Richtmyer, R. D., and K. W. Morton, Difference Methods for Initial Value Problems, (2nd Edition), Interscience, New York, 1967.

27. Forsythe, G. E., and W. R. Wasow, Finite-Difference Methods for Partial Differential Equations, Wiley, New York, 1967.

28. Lax, P. D., and B. Wendroff, "Difference Schemes for Hyperbolic Equations with High Order of Accuracy," Comm. Pure Appl. Math., Vol. 18, 1964.

29. Campbell, N. G., "Stability Analysis of a Difference Scheme for the Navier-Stokes Equations," Numer. Math., Vol. 14, 1970.

30. Brunson, R. J., and R. M. Wellek, " A Stable Explicit Method for Simultaneous Quasi-Linear Differential Equations," AIChE J., Vol. 17, No. 3, May 1971.

31. Lovin, J. K., "Lockheed-Huntsville Thermal Analyzer," LMSC-HREC D225095, Lockheed Missiles & Space Company, Huntsville, Ala., July 1972.

32. Feldman, K. T , "Review of the Literature on Sondhauss Thermoacoustic Phenomena," J. Sound Vib., Vol. 7, 1968, p. 78.

Appendix A

ONE-DIMENSIONAL THERMAL CONVECTION COMPUTER PROGRAM (TC1)

Appendix A

A.1 PROGRAM LOGIC

The TC1 program consists of three main blocks:

Input	Reads and prints all input data and initializes parameters
Calculation	Solves momentum, continuity, energy and state equations
Output	Prints convection solutions.

A block diagram of the program is shown in Fig. A-1.

The program is designed in subroutine form with a DRIVER program to control the subprogram calls. Figure A-2 is a flow chart of the TC1 DRIVER routine. The coding is entirely in standard third generation FORTRAN. It has been run on the Univac 1108 Exec 8 system, but can operate on any system having a FORTRAN IV or V compiler and at least 10K of core memory. No external storage devices are needed.

Problems using Model 1 or Model 2 (as described in Section 2) can be run with the TC1 program. The physical input data can be either in metric or English units. The program calculations are all performed in terms of dimensionless quantities (see Section 2) and the output is also in terms of dimensionless variables. All input is via cards which are punched according to the input guide which follows.

A.2 INPUT GUIDE

All input to the TC1 program is via punched cards. No tapes or drums are used. The input primarily consists of the following card groups.

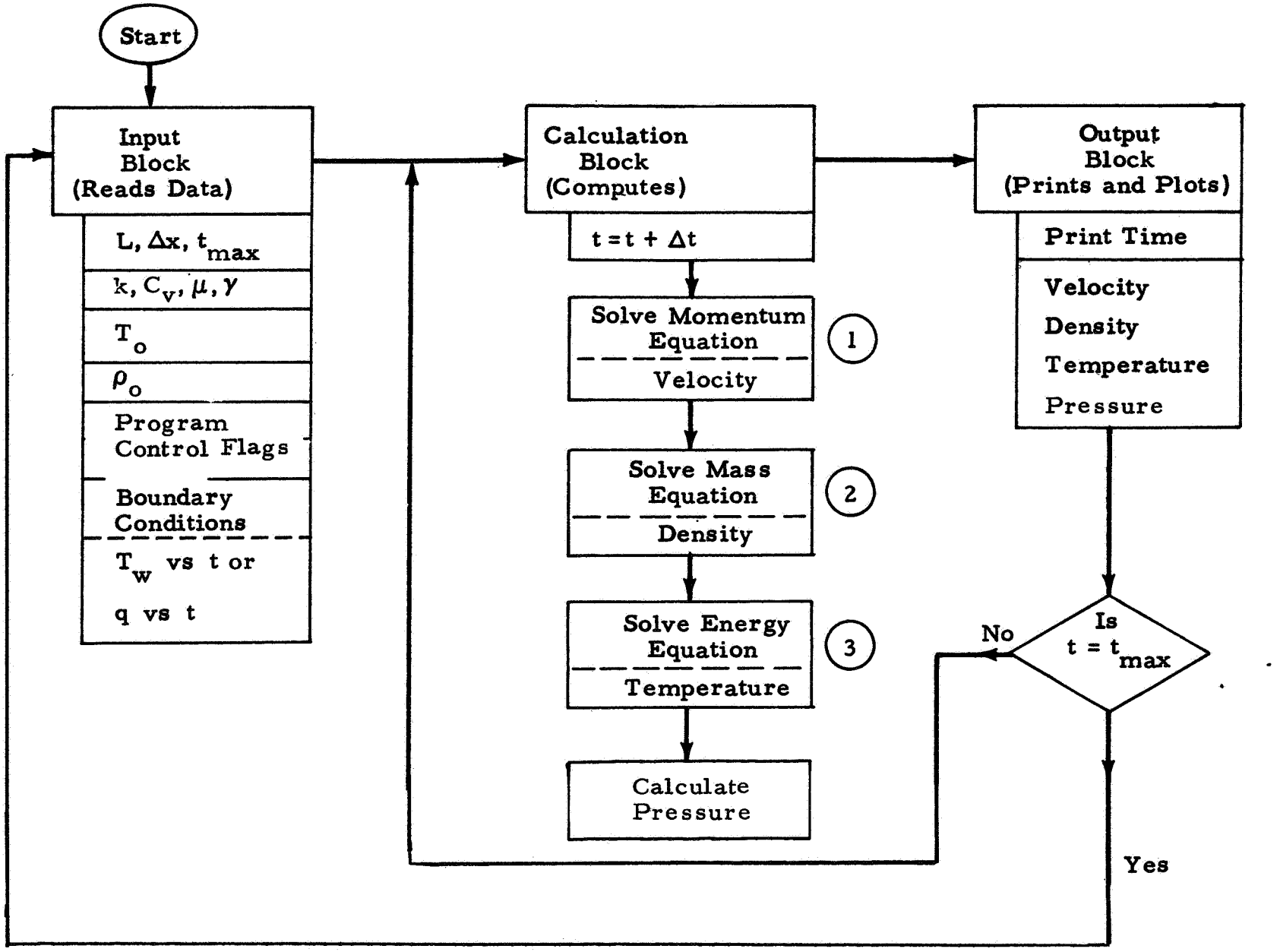

Fig. A-1 - Block Diagram for 1-D Thermal Convection Computer Program (TC1)

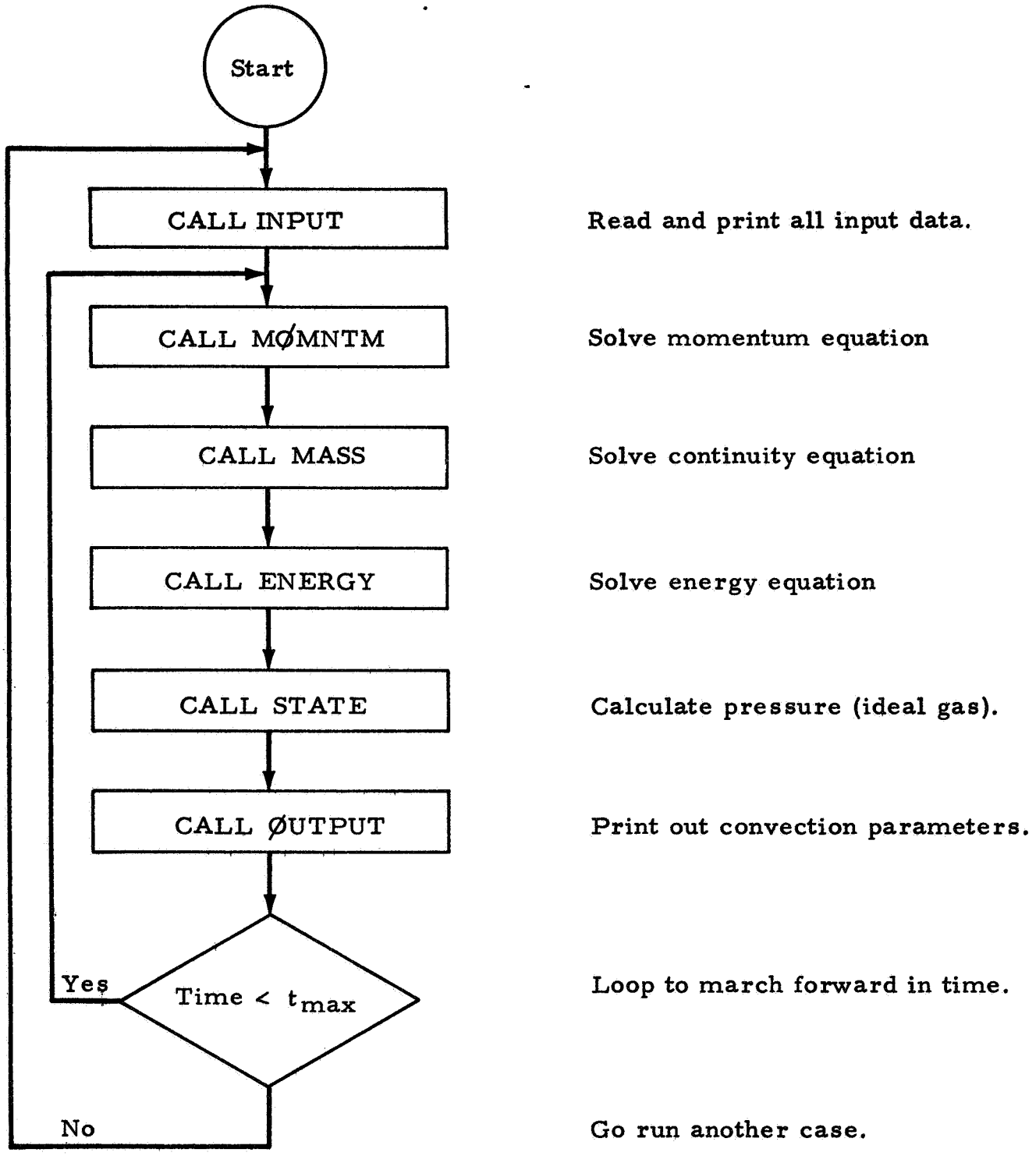

Fig. A-2 - Flow Chart of DRIVER Program for TC1

Card 1 - Title card

2 - Program control flags

3 - Physical parameters and initial conditions

4 - Thermal properties

5 - Boundary conditions

In addition, there are other optional cards as follows:

Card groups 6-7	Variable boundary condition tables
Card groups 8-11	Restart information
Card group 12	Normal run termination card.

Details of the input data, formats and options are now given.

CARD 1 Format (80A1)

Variable	Description
TITLE	Problem description card. Any FORTRAN characters can be used to identify the problem being run.

CARD 2 Format (14I5)

Variable	Description
NN	Number of nodes to be used in finite-difference grid (50 maximum, nominally 20).
NPRNT	Print control flag. Program will print out every NPRNT time steps.
ISTART	Restart flag. If ISTART = 1, program will run from the standard initial conditions. If ISTART = 2, profiles of temperature, density and velocity at a given time are read-in and used as initial conditions. This option allows restarting a problem if more time steps are needed or if program terminates due to "max-time."
ICOORD	Coordinate control flag. If ICOORD = 1, the inifinite flat plate model equations are used. If ICOORD = 2, the radial coordinate — concentric cylinder model equations are used.

CARD 2 (Cont'd) Format (14I5)

Variable	Description
IUNITS	Units control flag. If IUNITS = 1, metric units are assumed to be input. If IUNITS = 2, English units are assumed. The appropriate input units are shown with Cards 3, 4 and 7.
ITYPE	Flag to control the program flow. ITYPE = 1 runs the program in standard mode; the momentum, mass and energy equations are solved in full. ITYPE = 2 signals a conduction-only run. The energy equation with no convective terms is solved. This option can be used to compare the effects of convection on the temperature profile.

CARD 3 Format (8E10.0)

Variable	Description
XL	Distance L between the two plates (if ICOORD = 1) or radius L of outer cylinder (if ICOORD = 2), (cm or ft)
TZ	Initial isothermal absolute temperature T_o of fluid at rest, (^oK or ^oR).
RHOZ	Density ρ_o of fluid at temperature T_o and pressure P_o, (gm/cm^3 or lb/ft^3).
PZ	Initial pressure P_o ($dyne/cm^2$ or lb/ft^2). Either P_o or ρ_o can be input and the program will calculate the other from the ideal gas state equation.
DTIME	Dimensionless time step Δt. ($\Delta t = \Delta t' \sqrt{R' T'_o}/L'$) used to start the calculation. The program monitors the stability criterion and adjusts Δt to maintain stability.
TIMEMX	Dimensionless time at which the calculation terminates. ($t_{max} = t'_{max} \sqrt{R' T'_o}/L'$).
RZ	Radius of inner cylinder (heater) if ICOORD = 2. RZ should be zero if ICOORD = 1.
SCALE	Scale factor, s, (dimensionless) used to scale problem "time" to ease the small time step restriction (see Section 3.4).

CARD 4 Format (5E10.0)

Variable	Description
CONDZ	Thermal conductivity, k, of fluid, (dyne/sec ^{o}K or Btu/ft-sec-^{o}R).
VISCZ	Dynamic viscosity, μ, of fluid, (gm/cm-sec or lb/ft/sec)
CVZ	Specific heat at constant volume, C_v, of fluid (dyne-cm/gm-^{o}K or Btu/lb-^{o}R).
GAMMAZ	Ratio of specific heats, γ (dimensionless).
Z	Compressibility coefficient in equation of state (dimensionless). The present program can use any $0 < Z \leq 1$ in computing pressure from $P = \rho ZRT$

CARD 5 Format (I5, 2E10.0, I5)

Variable	Description
IBOUND	Control flag for boundary condition on $x = 0$ (or $r = r_o$) surface. IBOUND = ± 1 a specified temperature T_w is used. IBOUND = ± 2 a specified heat flux q_w is used. Positive values of IBOUND will cause a constant T_w or q_w to be used. A negative IBOUND allows tables of T_w or q_w versus time to be read-in and the boundary condition will be variable as a function of time (see Cards 6, 7).
TW	Dimensionless wall temperature to be applied to $x = 0$ (or $r = r_o$) surface. If IBOUND = +1 this TW will be used as a constant boundary condition; If IBOUND = -1 TW is computed by linear interpolation from the input table (Card 7).
QIN	Dimensionless heat flux ($q'L'/k'T'_o$) to be applied to $x = 0$ (or $r = r_o$) surface. If IBOUND = +2, this QIN will be used as a constant boundary condition; if IBOUND = -2, QIN is computed by linear interpolation from the input table (Card 7).
ITOP	Boundary condition control flag for $x = L$ surface. ITOP = 1, an isothermal surface (T_o) at $x = L$ will be used. If ITOP = 2 an adiabatic surface ($q = 0$) at $x = L$ will be used.

CARD 6 (Optional) Format (I5)

Variable	Description
NPT1	Number of pairs to be input in T_w versus time or q_w versus time tables. Input only if IBOUND is negative.

CARD GROUP 7 (Optional) Format (8E10.0)

Variable	Description
TABLE	Tables of wall temperature or wall heat flux versus time. IBOUND = -1 these are T_w versus time tables. IBOUND = -2 these are q_w versus time tables. The input is alternate values of time and T_w (or q_w); three pairs to a card until NPT1 pairs are read. (t_1, T_{w_1}, t_2, T_{w_2}, t_3, T_{w_3}). The times are in seconds and the temperatures are in ^oF or ^oC. The heat fluxes are in watts/cm^2 or Btu/ft^2-sec.

CARD GROUP 8 (Optional) Format (E15.7)

Variable	Description
TIME	Restart time. If ISTART = 2, this card is read, if ISTART = 1, do not input it. TIME is the dimensionless time at which the program is to be restarted.

CARD GROUP 9 (Optional) Format (5E15.7)

Variable	Description
T(I)	Temperature profile (I = 1, NN) at the time the run is to be restarted (dimensionless). These and the other restart profiles are to be punched from the printout at the point where the previous run stopped.

CARD GROUP 10 (Optional) Format (5E15.7)

Variable	Description
U(I)	Velocity profile for restart (see Group 9)

CARD GROUP 11 (Optional) Format (5E15.7)

Variable	Description
RHO(I)	Density profile for restart (see Group 9).

CARD GROUP 12 Format (80A1)

Variable	Description
TITLE	Run termination card. As many cases as desired can be run back-to-back simply by staking them. After the last case, a psuedo-title card is punched with the characters ENDRUN (Cols. 1-6). This causes a normal program stop.

A.3 SAMPLE CASE

The infinite parallel plate problem discussed in Section 4 is shown here as an example of the input and output formats of the TC1 program. A sample input is shown below.

INPUT CARDS

```
INFINITE PLATE PROBLEM  HELIUM  TW=2
   20 1000     1     1     1     1
  15.3      273.0       1.910F-4    0.0      0.05       1000.      0.0          1.0
  1.440F+4  1.875F-4    3.160F+7    1.666    1.0
     1    2.0        0.0            1
ENDRUN
```

A sample output is given in Fig. A-3. A printout of the input data is shown for checking the user input. A sample flow field is shown at one time point to illustrate the format. The meaning of the major variables are the same as described in the input guide.

INFINITE PLATE PROBLEM HELIUM TW=2

NN= 20 NPRNT= 1000 ISTART= 1 ICOORD= 1 IUNITS= 1 ITYPE= 1

L= .1530+02 TZ= .2730+03 RHOZ= .1910-03

DTIME= .5000-01 TIMEMX= .1000+04 RZ= .0000 SCALE= .1000+01

CONDZ= .1440+05 VISCZ= .1875-03 CVZ= .3160+08 GAMMAZ= .1666+01 Z=1.0

IBOUND= 1 TW= .200000+01 QIN= .000000 ITOP= 1

FR= .3832+06 RE= .1181+07 PR= .6855+00 PZ= .1097+07 SQRTZ= .7580+05

TIME= .500000+03 REAL TIME = .100925+00 TW= .200000+01 PAVG= .127118+01
NU= .230410+01 SUMR= .200000+02 SUMT= .132585+01

NODE	X	T	U	RHO	P
1	.2500000-01	.1942397+01	-.8239886-03	.6483603+00	.1259373+01
2	.7500000-01	.1840845+01	-.2403343-02	.6844492+00	.1259965+01
3	.1250000+00	.1744823+01	-.3959586-02	.7228322+00	.1261215+01
4	.1750000+00	.1655031+01	-.5387975-02	.7631298+00	.1263003+01
5	.2250000+00	.1571342+01	-.6426457-02	.8053893+00	.1265542+01
6	.2750000+00	.1493457+01	-.7371314-02	.8493404+00	.1268453+01
7	.3250000+00	.1421384+01	-.7786046-02	.8947630+00	.1271802+01
8	.3750000+00	.1355231+01	-.7825852-02	.9408699+00	.1275096+01
9	.4250000+00	.1295709+01	-.7380555-02	.9865452+00	.1278275+01
10	.4750000+00	.1243717+01	-.6387115-02	.1029687+01	.1280639+01
11	.5250000+00	.1200484+01	-.4926197-02	.1068157+01	.1282304+01
12	.5750000+00	.1166125+01	-.3186228-02	.1099901+01	.1282622+01
13	.6250000+00	.1139036+01	-.1507046-02	.1125248+01	.1281699+01
14	.6750000+00	.1116864+01	.1878481-03	.1145799+01	.1279701+01
15	.7250000+00	.1097324+01	.1483925-02	.1163415+01	.1276642+01
16	.7750000+00	.1079282+01	.2296421-02	.1179824+01	.1273362+01
17	.8250000+00	.1061791+01	.2502348-02	.1195890+01	.1269773+01
18	.8750000+00	.1044480+01	.2217103-02	.1212756+01	.1266699+01
19	.9250000+00	.1026929+01	.1548746-02	.1231184+01	.1264338+01
20	.9749999+00	.1008403+01	.5216916-03	.1252490+01	.1263128+01

Fig. A.3 – Sample Output of TC1 Program

Appendix B

DUFORT-FRANKEL NUMERICAL SCHEME FOR THERMAL CONVECTION

APPENDIX B

The numerical scheme presented in Section 3 of this report has first-order accuracy truncation error in the time variable. For some fluid mechanics applications this order of accuracy is insufficient to produce meaningful results. However, for the thermal convection problems being analyzed here, these first-order methods should be sufficiently accurate. In order to provide a check on the accuracy of the first order method, a Dufort-Frankel (Ref. B-1) algorithm was devised and coded. The classical Dufort-Frankel scheme was chosen for comparison for the following reasons:

- Second-order accuracy truncation error in both time and distance
- Simplicity of programming
- The smallest computer/real time ratio of the five schemes tested by Torrance (Ref. B-1)

The form of the conservation equations and their finite difference representations are shown in Fig. B-1 to B-3. These finite differences incorporate the same node-centered spatial mesh used in the original TC1 program.

The TC1 explicit technique is utilized as a starter for this multi-time step scheme. Solutions are marched out in time from the known initial conditions. The same logic, schematically accounted for in Appendix A was used for the Dufort-Frankel scheme as in TC1 except that a CALL START block was inserted immediately following the CALL INPUT block.

The Dufort-Frankel program was applied to the sample problem of Larkin (Ref. B-2) and the results compared to those of the Lockheed TC1 program.

Temperature profiles for the sample problem are compared in Fig. B-4. These profiles are practically identical except that the Dufort-Frankel temperature gradient at the cool wall is more realistic $\left(\left.\frac{\partial T}{\partial x}\right|_{x=1} < 0\right.$ rather than positive$\Big)$. This was a relatively minor change, however, as seen in Fig. B-4 The velocity (u) and pressure (P) profiles were also very similar, viz.,

	TC1	Dufort-Frankel
u_{max}	$0.018\sqrt{RT_o}$	$0.017\sqrt{RT_o}$
Period of Velocity Waves	10^{-3} sec	10^{-3} sec
$\left.\frac{P_{avg}}{P_o}\right\|_{t=2000}$	1.34	1.33

Thus, the TC1 and Dufort-Frankel solutions of the sample problem are in very close agreement. This is significant, since the two solution techniques use entirely different numerical approximations, and both yield similar results. The agreement indicates that the Lockheed velocity profiles rather than the Larkin (Ref. B-2) and Thuraisamy (Ref. B-3) results, are more realistic, since Larkin and Thuraisamy used essentially identical numerical techniques. Furthermore, the maximum velocity attained in TC1 and D-F solutions seem more realistic from a physical viewpoint because Larkin and Thuraisamy's maximum velocities were 1/5 the speed of sound whereas those of Lockheed were only 1/50 of sonic.

In conclusion, the second-order accurate Dufort-Frankel method has produced essentially the same results as the first-order method defined in Section 3. The accuracy of the first order method is thus established numerically and has been used for all calculations presented in the main text of this report.

Momentum Equation

$$\frac{\partial u}{\partial t} = -\frac{g}{Fr} - \frac{\partial}{\partial x}\left(\frac{u^2}{2}\right) - \frac{1}{\rho}\frac{\partial P}{\partial x} + \frac{4\mu}{3\,Re\,\rho}\frac{\partial^2 u}{\partial x^2}$$

Finite Difference Form

$$u_i^{n+1} = \frac{1}{(1+A)}\left[\begin{array}{l} u_i^{n-1} - \frac{2\Delta t\, g}{Fr} - \frac{\Delta t}{(2+a)\Delta x}\,\delta_x\left(\frac{u^2}{2}\right)_i^n \\ \\ -\frac{\Delta t}{\rho_i^n \Delta x}\,\delta_x (P)_i^n + A\,\delta_x^2 (u)_i^n \end{array}\right]$$

where $A = \dfrac{8\mu\Delta t}{3\,Re\,\rho_i^n (\Delta x)^2}$ $\qquad a \geq 0$

Difference Equations

$$\delta_x\left(\frac{u^2}{2}\right)_i^n = (u_{i+1}^n)^2 + a\,u_i^n (u_{i+1}^n - u_{i-1}^n) - (u_{i-1}^n)^2 \qquad i = 2, \ldots, k-1$$

$$\delta_x\left(\frac{u^2}{2}\right)_1^n = (u_2^n)^2 + a\,u_1^n (u_2^n + u_1^n) - (u_1^n)^2$$

$$\delta_x\left(\frac{u^2}{2}\right)_k^n = (u_k^n)^2 - a\,u_k^n (u_k^n + u_{k-1}^n) - (u_{k-1}^n)^2$$

$$\delta_x (P)_i^n = P_{i+1}^n - P_{i-1}^n \qquad i = 2, \ldots, k-1$$

$$\delta_x (P)_1^n = -3P_1^n + 4P_2^n - P_3^n \qquad \delta_x (P)_k^n = 3P_k^n - 4P_{k-1}^n + P_{k-2}$$

$$\delta_x^2 (u)_i^n = u_{i+1}^n - u_i^{n-1} + u_{i-1}^n \qquad i = 2, \ldots, k-1$$

$$\delta_x^2 (u)_1^n = u_2^n - \frac{3}{2}\,u_1^{n-1}$$

$$\delta_x^2 (u)_k^n = u_{k-1}^n - \frac{3}{2}\,u_k^{n-1}$$

Fig. B-1 - Finite Difference Form of Momentum Equation (Dufort-Frankel)

Continuity Equation

$$\frac{\partial \rho}{\partial t} = - \frac{\partial}{\partial x} (\rho u)$$

Finite Difference Form

$$\rho_i^{n+1} = \rho_i^n - S \left[\theta \delta_x (\rho u)_i^{n+1} + (1 - \theta) \delta_x (\rho u)_i^n \right]$$

where θ = constant, $1/2 \leq \theta \leq 1$, $S = \Delta t / 2 \Delta x$

Difference Equations

$$\delta_x (\rho u)_i^n = \rho_{i+1}^n u_{i+1}^n - \rho_{i-1}^n u_{i-1}^n \qquad i = 2, \ldots k-1$$

$$\delta_x (\rho u)_1^n = \rho_1^n u_1^n + \rho_2^n u_2^n \qquad \delta_x (\rho u)_k^n = - \rho_k^n u_k^n - \rho_{k-1}^n u_{k-1}^n$$

Resulting Tri-Diagonal System

$$A_i \rho_{i-1}^{n+1} + B_i \rho_i^{n+1} + C_i \rho_{i+1}^{n+1} = D_i \qquad i = 1, \ldots, k$$

where

$A_i = - S u_{i-1}^{n+1}$ $\qquad$ $C_i = S u_{i+1}^{n+1}$

$B_i = 1.0$ $\qquad$ $D_i = \rho_i^n - S(1-\theta) \delta_x (\rho u)_i^n$

$A_1 = 0.0$ $\qquad$ $A_k = - S \theta u_{k-1}^{n+1}$

$B_1 = 1 + S\theta u_1^{n+1}$ $\qquad$ $B_k = 1 - S \theta u_k^{n+1}$

$C_1 = S \theta u_2^{n+1}$ $\qquad$ $C_k = 0.0$

Fig. B-2 - Finite Difference Form of Continuity Equation (Larkin)

Energy Equation

$$\frac{\partial T}{\partial t} = - u \frac{\partial T}{\partial x} - (\gamma - 1) T \frac{\partial u}{\partial x} + \frac{k\gamma}{\rho C_V \mathrm{Re}\,\mathrm{Pr}} \frac{\partial^2 T}{\partial x^2}$$

Finite Difference Form

$$T_i^{n+1} = \frac{1}{(1+B)} \left[\begin{array}{l} T_i^{n-1} - \frac{\Delta t}{\Delta x} u_i^n \delta_x (T)_i^n \\ \\ - \frac{(\gamma - 1)\Delta t}{\Delta x} T_i^n \delta_x (u)_i^n - B \delta_x^2 (T)_i^n \end{array} \right]$$

where $B = \dfrac{2 k \gamma \Delta t}{C_V \mathrm{Re}\,\mathrm{Pr} (\Delta x)^2 \rho_i^n}$

Difference Equations

$$\delta_x (T)_i^n = T_{i+1}^n - T_{i-1}^n \qquad i = 2, \ldots, k-1$$

$$\delta_x (T)_1^n = 2 (T_1^n - T_w) \qquad \delta_x (T)_k^n = 2 (T_o - T_k^n)$$

$$\delta_x (u)_i^n = u_{i+1}^n - u_{i-1}^n \qquad i = 2, \ldots, k-1$$

$$\delta_x (u)_1^n = u_1^n + u_2^n \qquad \delta_x (u)_k^n = - u_{k-1}^n - u_k^n$$

$$\delta_x^2 (T)_i^n = T_{i+1}^n - T_i^{n-1} + T_{i-1}^n \qquad i = 2, \ldots, k-1$$

$$\delta_x^2 (T)_1^n = T_2^n - 3/2\, T_1^{n-1} + 2 T_w$$

$$\delta_x^2 (T)_k^n = T_{k-1}^n - 3/2\, T_k^{n-1} + 2 T_o$$

Fig. B-3 - Finite Difference Form of Energy Equation (Dufort-Frankel)

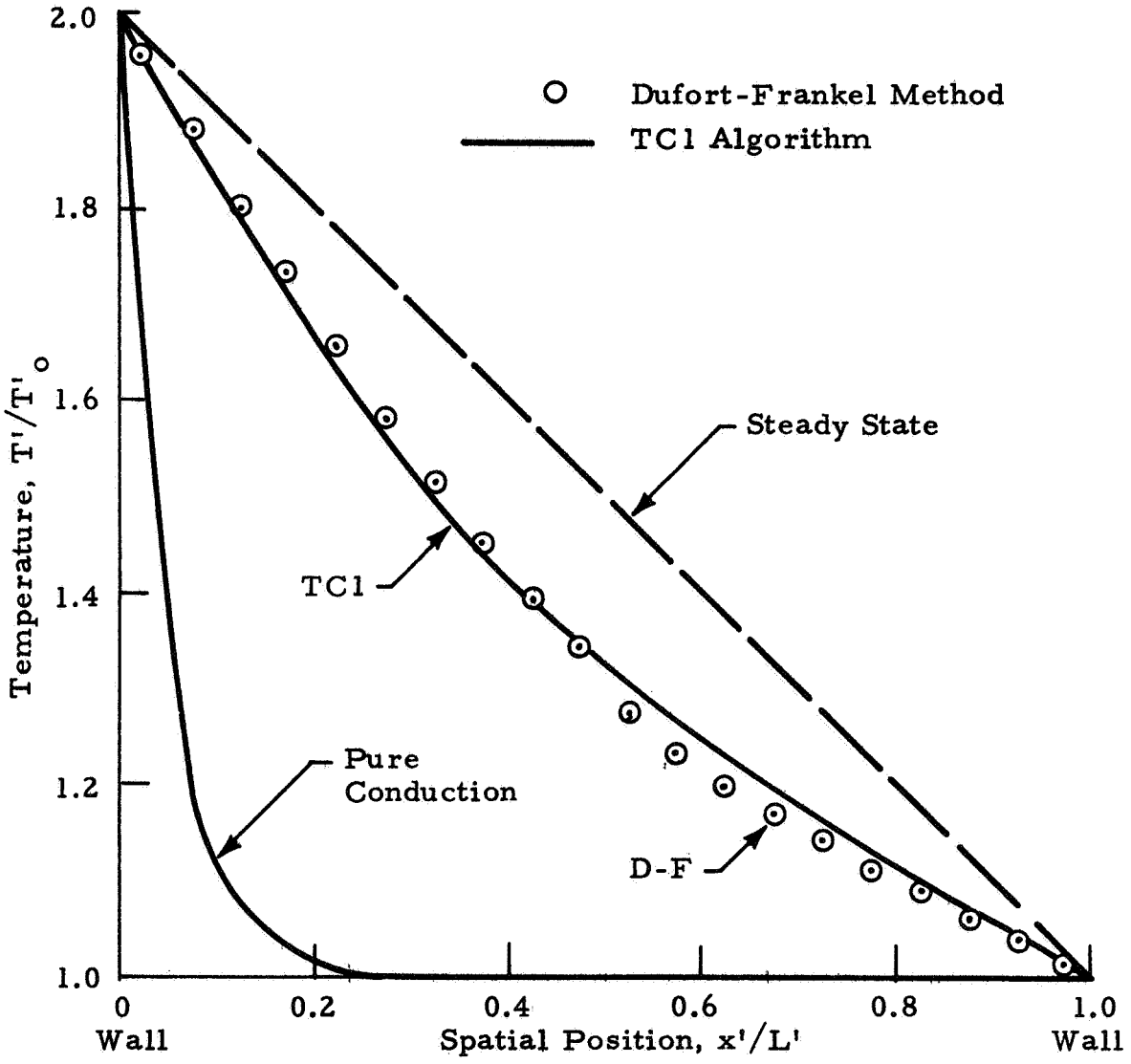

Fig. B-4 - Temperature vs Position at 0.2 Seconds Comparing Dufort-Frankel and TC1

REFERENCES

B-1. Torrance, K. E., "Comparison of Finite-Difference Computations of Natural Convection," J. Research, National Bureau of Standards, Vol. 72B, No. 4, October 1968.

B-2. Larkin, B. K., "Heat Flow to a Confined Fluid in Zero Gravity," Progress in Astronautics and Aeronautics, Thermophysics of Spacecrafts and Planetary Bodies, Edited by G. B. Heller, Vol. 20, 1967.

B-3. Thuraisamy, V., "Thermodynamic Flow of Supercritical Oxygen in Zero Gravity," Bellcomm TM 72-1022-1, Bellcomm, Inc., Washington, D. C., March 1972.

*U.S. GOVERNMENT PRINTING OFFICE: 1973-739-028/41

NATIONAL AERONAUTICS AND SPACE ADMINISTRATION
WASHINGTON, D.C. 20546

OFFICIAL BUSINESS
PENALTY FOR PRIVATE USE $300

SPECIAL FOURTH-CLASS RATE BOOK

POSTAGE AND FEES PAID
NATIONAL AERONAUTICS AND SPACE ADMINISTRATION
451

U.S.MAIL

POSTMASTER. If Undeliverable (Section 158 Postal Manual) Do Not Return

"The aeronautical and space activities of the United States shall be conducted so as to contribute . to the expansion of human knowledge of phenomena in the atmosphere and space. The Administration shall provide for the widest practicable and appropriate dissemination of information concerning its activities and the results thereof."

—NATIONAL AERONAUTICS AND SPACE ACT OF 1958

NASA SCIENTIFIC AND TECHNICAL PUBLICATIONS

TECHNICAL REPORTS: Scientific and technical information considered important, complete, and a lasting contribution to existing knowledge.

TECHNICAL NOTES: Information less broad in scope but nevertheless of importance as a contribution to existing knowledge.

TECHNICAL MEMORANDUMS: Information receiving limited distribution because of preliminary data, security classification, or other reasons. Also includes conference proceedings with either limited or unlimited distribution.

CONTRACTOR REPORTS: Scientific and technical information generated under a NASA contract or grant and considered an important contribution to existing knowledge.

TECHNICAL TRANSLATIONS: Information published in a foreign language considered to merit NASA distribution in English.

SPECIAL PUBLICATIONS: Information derived from or of value to NASA activities. Publications include final reports of major projects, monographs, data compilations, handbooks, sourcebooks, and special bibliographies.

TECHNOLOGY UTILIZATION PUBLICATIONS: Information on technology used by NASA that may be of particular interest in commercial and other non-aerospace applications. Publications include Tech Briefs, Technology Utilization Reports and Technology Surveys.

Details on the availability of these publications may be obtained from:

SCIENTIFIC AND TECHNICAL INFORMATION OFFICE

NATIONAL AERONAUTICS AND SPACE ADMINISTRATION

Washington, D.C. 20546